From cell size and first principles to structure and function of unicellular plankton communities

K.H. Andersen and A.W. Visser
Center for Ocean Life,
Natl. Inst. for Aquatic Resources, Technical University of Denmark,
Bygning 202, Kgs. Lyngby, Denmark. E-mail: khand@dtu.dk.

May 25, 2022

Highlights

- Review of how cell size affects resource uptake, losses, and metabolism.
- Derivation of most cell-level parameters from first principles.
- Closed-form solutions of limiting resources and size spectrum
- Scaling from cell-level processes to size structure and ecosystem functions.

Abstract

Here we review, synthesize, and analyse the size-based approach to model unicellular plankton cells and communities. We connect cell-level processes to cell size and to first principles of diffusion, geometry, and fluid mechanics. We scale cell-level processes up to the plankton community size distribution to show that first principles determine overall plankton community structure and function. We first review how cell size influences processes of the individual the cell: uptake of dissolved nutrients, phototrophy, phagotrophy, and metabolism. We parameterise processes primarily from first principles using a synthesis of existing data only when needed, and show how these processes determine minimum and maximum cell size and limiting resource concentrations. The cell level processes scale directly up to the structure and function of the entire unicellular plankton ecosystem. The structure is described by the Sheldon size spectrum and by the emergent trophic strategies. We develop an analytical approximate solution of the biomass size spectrum and show how the trophic strategies depend on the resource environment. The functions of the plankton community are the production, respiration and losses, and carbon available to production of higher trophic levels. We finally

discuss strengths and limitations of size-based representations and models of plankton communities.

Keywords— Cell size, traits, plankton, DOC, Sheldon, mixotrophy

1 Introduction

Our understanding of the physical world is rooted in "first principles". First principles are the rules and equations whose validity are considered fundamental and unchanging. First principles include fluid mechanics, conservation laws, diffusion principles, stoichiometry, and chemical reaction kinetics. Models of ecosystems do not have recourse to such first principles. Nevertheless, the individual organisms are constrained by first principles that are manifested at all scales of life, from the reaction kinetics and topology of life's fundamental molecules, the physical limitations of functions of the cells, the circulatory systems, and the geometry of the body plan. One aspect of life where first principle constraints are most evident is in relations to the size of individual organisms (Haldane, 1926; Andersen et al., 2016). Here we attempt to go beyond the individual organism and scale to ecosystem structure and function. We use unicellular planktonic life as the example.

Unicellular plankton is an incredibly diverse group of organisms. Taxonomically they represent four domains of life: archaea, bacteria, algae and protozoa. Plankton size spans 8 orders of magnitude in mass, the same range as between a beetle and an elephant. Functionally, unicellular planktonic ecosystems show the entire range of trophic strategies of primary producers (phytoplankton), grazers and predators (zooplankton), and decomposers (bacteria). The unicellular planktonic food web drives the fast turnover of inorganic dissolved matter in the oceans, half the global primary production, the main carbon flux from the photic zone, and the turn-over of inorganic and organic matter. All metazoans – multicellular plankton, jellies, fish, benthic organisms, and marine mammals – rely on the surplus production from the unicellular plankton food web (Ryther, 1969; Stock et al., 2017). Without the unicellular food web, macroscopic life in the oceans would be extremely impoverished.

The difficulty of observing and experimenting with unicellular plankton food webs have put models in central position, not just for predictions of responses to changes, but also for understanding the structure and function of the ecosystems. Any ecosystem model needs to choose how to represent the diversity of organisms. The classic food web models approach resolves each and every population and their interactions with other populations. This approach only works for smaller isolated ecosystems, and it is difficult to apply to unicellular plankton where we rarely have a clear overview of the full taxonomic diversity or even species differences. Plankton models instead describe diversity by lumping species into distinct functional groups. The simplest groups are between phytoplankton and zooplankton, with phytoplankton representing all phototrophic organisms and zooplankton their grazers (Franks, 2002). Despite the simplicity of such "NPZ" models, they remarkably successfully captures the main features of seasonal succession (Evans and Parslow, 1985; Fasham et al., 1990; Anderson et al., 2015) and global patterns of production (e.g. Palmer and Totterdell, 2001). However, the success is contingent on model parameters being tuned to the observations themselves. In this way, parameters of each group is tuned to

represent the physiology of the dominant species in the group. However, when conditions change, other species with different parameters enters and the model no longer represents the new ecosystem (Franks, 2009). This parameter tuning therefore reduces our confidence in the model's ability to reproduce ecosystem dynamics when conditions change outside the model's tuning envelope.

A further elaboration of plankton diversity is achieved by breaking the trophic groups into further functional groups (Anderson, 2005; Quere et al., 2005; Hood et al., 2006). The functional groups are often aligned with dominant taxonomic groups including coccolithophores, dinoflagellates, ciliates, and diatoms. While the functional-group approach introduce additional flexibility and accuracy it does so at the price of increased complexity and additional parameters. Each group still represents a huge diversity of organisms – for example, the size range of diatoms spans from a few tens to 10^7 cubic micrometers – and parameters for each group are still tuned to represent the dominant species in the modelled region. While the introduction of further realism improves the models fit to observations it also leads to a complexity trap with a proliferation of state variables and parameters.

Size-based models break free of the complexity trap of functional groups by using size groups that represents all cells in a given size range regardless of their taxonomic affiliation. Technically, each size group is modelled largely in the same way as a functional groups. The main difference is that the parameters are not independently determined for each size group. Instead, parameters follow from a smaller set of scaling coefficients and exponents that apply to all sizes. In this manner size models are flexible with respect to the number of state variable while retaining a small set of parameters that is – at least in theory – generally valid.

Size-based models of plankton have a long history (Armstrong, 1994; Moloney and Field, 1989; Baird and Suthers, 2007; Stock et al., 2008; Banas, 2011; Negrete-García et al., 2022). Size-based concepts are now increasingly used in bio-geo-chemical models to increase the diversity within functional groups according to size (Terseleer et al., 2014; Ward et al., 2018; Stock et al., 2014). Most size-based models retain the distinction of functional trophic groups by operating with separate phyto- and zooplankton size distributions. A recent strand is purely size-based models where the only difference between cells are their size and no distinction between trophic strategy is imposed (Ward and Follows, 2016; Ward et al., 2018; Ho et al., 2020; Chakraborty et al., 2020). Such models completely forgo taxonomic-oriented assumptions about the function of the modelled groups (Andersen et al., 2015). All functional differences between size groups and of the community are emergent properties of the model. Size-based models mostly rely on empirical relationships between size and half-saturation coefficients, etc. This approach ensures a good fit with observations. Here, we instead try to establish the fundamental mechanisms and strive to determine parameters from fundamental principles.

There are other reasons for using cell size as the governing axis of diversity. It is now well documented that many of the fundamental rates and processes within plankton scales with cell size (Finkel et al., 2010; Marañón, 2015): affinities for nutrients (Edwards et al., 2012) or light (Taguchi, 1976; Edwards et al., 2015), maximum bio-synthesis rates and respiration rates (Kiørboe and Hirst, 2014), clearance rates (Kiørboe and Hirst, 2014), predator-prey mass ratios (Hansen et al., 1994) and predation risk from larger organisms (Hirst and Kiørboe, 2002). Importantly, many of those scaling relations emerge

from fundamental physical limitations due to geometry (light affinity), diffusion (affinity for dissolved organic matter), and fluid mechanics (sinking: Stokes' law, or feeding (Nielsen et al., 2017)). In other words: the parameters are constrained by first principles from geometry or classical physics. A further advantage of size-based models is the conceptual simplicity that comes from being based on a general description of a single cell. The simplicity extends to the implementation, which only needs a small parameter set. These advantages make size-based descriptions appealing to add diversity within a functional group (Terseleer et al., 2014; Stock et al., 2014) or for the full model structure.

There exist an abundance of reviews on the empirical relationships between cell size and various processes (Marañón, 2015; Edwards et al., 2012; Finkel et al., 2010; Hansen et al., 1994; Kiørboe and Hirst, 2014; Hillebrand et al., 2021). They tend to focus on phytoplankton and upon describing size-relations as a single power-law function. However, in many cases there are more than one underlying physical process at play. This means that there are transitions between one power-law relation and another, e.g., between nutrient diffusion and surface uptake (Armstrong, 2008) or between maximum synthesis rates and nutrient uptake (Ward et al., 2016). Such transitions at characteristic sizes often lead to important transition in the ecosystem structure (Andersen et al., 2016), for example between phototrophs, mixotrophs, and heterotrophs (Andersen et al., 2015). Identifying characteristic sizes where there is a cross-over between two power-law relations is therefore even more important for ecosystem structure and function than the power-law relations themselves.

Here we synthesize existing knowledge of size-based relationships for unicellular plankton, from bacteria to zooplankton. Our aim is to identify the first principles responsible for the size-based relations, thereby tying parameters to physical and chemical processes and geometry. We show how size-based relationships determine community-level patterns of biodiversity and ecosystem function: the viable size-range, competition, biomass size structure, ecosystem primary and secondary production, and trophic efficiencies. By focusing on the processes related to cell size, we show the power of these relations for determining community-level patterns and ecosystem functions. The review is organised in four parts. First we review the relations related to resource uptake, losses, and biosynthesis of a cell, including the theory the links these processes to first principles. Second, we exploit the simple form of the size-based relations to derive closed-form solutions for the smallest and larges cell sizes, and for the limiting resources. Third, we scale from the cells to the entire community size distribution and trophic strategy. We derive a scaling solution of the biomass size distribution and explore the trophic strategies and compare with simulations of the size-based model in a chemostat. Finally, we derive ecosystems functions, including production, and show how the plankton community responds to predation by higher trophic levels or changes in temperature. While our aim is not to make a perfect bio-geochemistry we nevertheless show that the model gives reasonable predictions of biomass and production. Overall, our synthesis highlights the importance of fundamental first principles for constraining the functions of unicellular plankton communities.

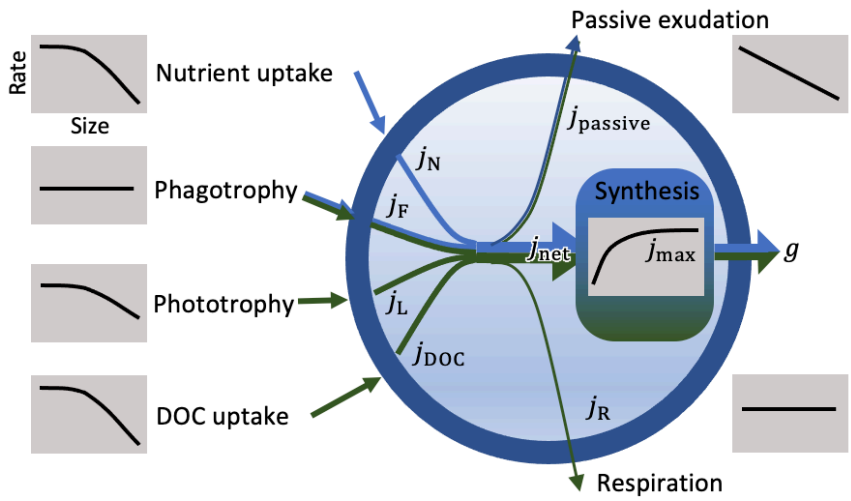

Figure 1: Sketch of the fluxes of nutrients (blue) and carbon (green) in and out of a cell. The grey insets sketches the size-dependency of each rate. Uptakes of nutrients j_{N}, food j_{F}, photoharvesting j_{L}, and dissolved organic carbon j_{DOC} are subjected to losses from respiration j_{R} and passive exudation j_{passive} before they are synthesised with a maximum rate j_{max}. The end result is the division rate g.

2 Effects of cell size on fundamental rates: resource uptake, losses, and biosynthesis

Ecosystem dynamics occur when individual cells acquire and process resources, eventually leading to cell division. This section reviews how cell size determines the uptakes of resources: dissolved nutrients, inorganic carbon through photoharvesting, dissolved organic carbon, and feeding on smaller organisms, and how the uptakes are determined by first principles. Some of the acquired resources are lost through passive exudation or used for respiration. The remaining resources are used for biosynthesis (Fig. 1). First, though, we discuss the measures of cell size.

2.1 Measures of cell size

The size of a cell can be measured in two ways: by its physical size – radius or volume – or by its mass, e.g., mass or moles of carbon or nitrogen. There is no universally optimal measure; for some processes physical size is most relevant, for others it is the mass, and for others both measures of size. For example, the settling velocity due to Stokes' law is determined by both the physical size and the mass of the cell. Physical size is mostly

used to describe limitations due to geometry, e.g., surface limitation, while mass is used to describe metabolism and the energy and mass budgets of the cell.

Conversion between physical size (equivalent spherical radius r) and mass of substance X, m_X for spherical cells is simply:

$$m_{\mathrm{X}} = \rho_{\mathrm{C}:X}\rho\frac{4}{3}\pi r^3 \;\Leftrightarrow\; r = \left(\frac{3m_{\mathrm{X}}}{4\rho_{\mathrm{C}:X}\rho}\right)^{1/3}, \tag{1}$$

where ρ is the carbon density (carbon mass per volume) and $\rho_{\mathrm{C}:X}$ is the elemental mass ratio between carbon and X.

In the following, mass is considered as carbon mass and the subscript C is suppressed $m = m_{\mathrm{C}}$. For the theoretical calculations we use a density of $\rho = 0.4 \cdot 10^{-6}$ µgC/µm^3 and Redfield elemental ratios. When working with data the conversion between physical size and mass needs to account for differences in shape and density. In particular diatoms are special due to their vacuole which lowers their density. We use the compilation of Menden-Deuer and Lessard (2000) that explicitly distinguishes between diatoms and other protists.

Not all of the cell mass m is actually available for functions of biosynthesis (ribosomes), light harvesting (chloroplast) etc. The cell wall itself takes up fraction of the cell mass (Raven, 1994; Marañón, 2015), and for small cell this fraction can severely limit the available functional mass. For a spherical cell the fraction of the cell used by the wall is approximately:

$$\nu = 3\frac{\delta}{r}, \tag{2}$$

where $\delta \approx 50$ nm is the thickness of the cell wall. The effective functional mass is therefore $m(1-\nu)$.

2.2 Resource uptake

Cells take up resources through three mechanisms: diffusive uptake of dissolved organic carbon (DOC) and inorganic matter (N), photoharvesting of light (L), and phagotrophic uptake of particulate matter (F). The potential uptake of resource X is proportional to the resource concentration:

$$j_X = a_X(m)X\rho_{\mathrm{C}:X}, \quad \text{for } X \in \{\mathrm{DOC,\ N,\ L,\ or\ F}\} \tag{3}$$

where j_X is the mass specific flux (in units of g_C/g_C/time), a_X is the mass specific affinity (volume/day/g_C), X is the resource in units of X per volume, and $\rho_{\mathrm{C}:X} = \rho_{\mathrm{C:N}}$ is the C:N ratio for diffusive uptake of nutrients. By multiplying with the fixed C:N ratio all the fluxes are measured in the same units and are therefore directly comparable.

The affinity is determined by the encounter with the resource and by the cell's investment in resource uptake capacity. The encounter is determined by physical processes of diffusion, self-shading, and fluid dynamics. For all resource uptakes, the mass-specific affinity is constant or decreases with size, as we will show below. The limitation due to uptake capacity is relevant when the cell encounters abundant amounts of the resource but is unable to process it all by its uptake machinery, e.g., porters for diffusive uptake, light

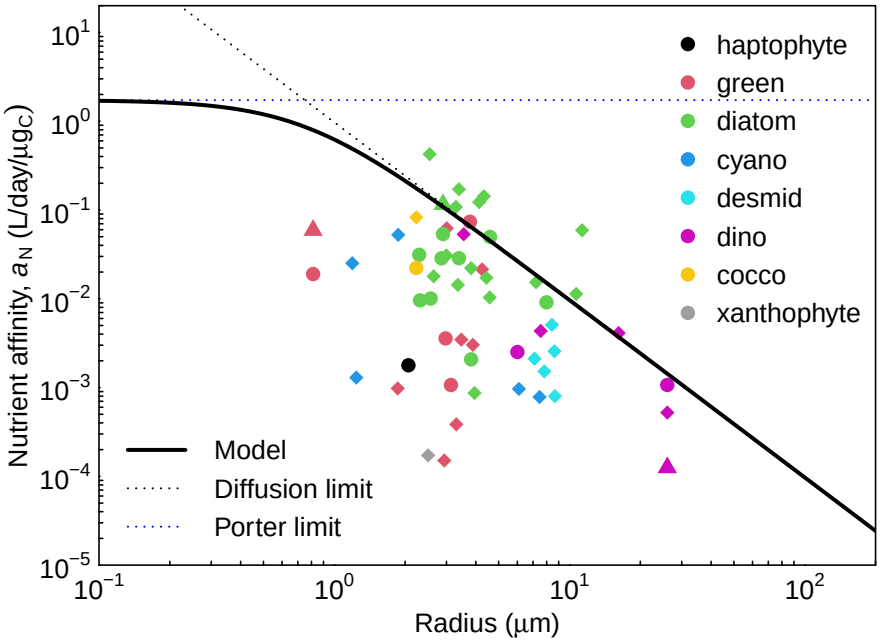

Figure 2: Specific nutrient affinity (a_{N}) as a function of radius. Triangles: ammonium uptakes; circles: nitrate uptake; diamonds: phosphorous uptake. The dotted lines are the theoretical maximum affinity due to diffusion limitation and porter limitation. The solid line is a fit-by-eye to radius where porter limitation becomes important, around $r_D^* = 2\mu\mathrm{m}$. Data from Edwards et al. (2015). Conversions between volume and mass are done using the relations in Menden-Deuer and Lessard (2000).

harvesting machinery, or phagotrophic assimilation. Uptake limitation is most prominent for small cells that have high affinities, leading to a higher encounter that they can process. Small cells can compensate by higher investments in the resource uptake machinery (Chakraborty et al., 2017). As investments scales with the mass of the cell, the uptake limitation of mass-specific affinity is independent of cell mass. Small cells therefore have limited ability to increase their uptake capacity, and their affinity will be limited by uptake capacity. The affinity then has two size-scaling regimes: for small sizes the affinity is independent with size (uptake limitation), and for larger sizes it is constant or declining with size (encounter limitation).

The processes that determine encounter and uptake capacity, and how they scale with cell size, depend on the type of resource.

2.2.1 Uptake of dissolved matter; theory and data

The theory behind uptake of dissolved matter is well developed, reviewed by Fiksen et al. (2013). Nutrient uptake is limited by three processes: the rate at which dissolved molecules diffuse towards the cell, the rate at which nutrients are transported across the cell wall by porters, and the capacity of the cell to utilize nutrients in biosynthesis.

The encounter with molecules is determined by the rate of diffusion towards the cell with a mass-specific affinity (Pasciak and Gavis, 1974):

$$a_{\mathrm{D}} = \frac{3D}{\rho} r^{-2} = \alpha_{\mathrm{D}} r^{-2}, \tag{4}$$

where D is the diffusivity of the dissolved molecules, ρ is the cell carbon density, and r is the cell radius. However, at small cell radius, mass specific affinity saturates as uptake becomes limited by either the number and capacity of porters, or by the cells' ability to process incoming nutrients. The functional form of the mass-specific affinity for dissolved nutrients can be approximated as:

$$a_{\mathrm{D}}(m) = \alpha_{\mathrm{D}} r^{-2} \frac{1}{1 + (r/r_D^*)^{-2}} \tag{5}$$

where r_{D}^* is the cell size at the cross-over between uptake (porter/processing) limitation and diffusion limitation. Small cells $d \ll r_{\mathrm{D}}^*$ are porter/processing limited and have a constant affinity $a_{\mathrm{D}} = 4\pi D/r_D^{*2}$ while larger cells, $d \gg r_D^*$ are diffusion limited with $a_X = 4\pi D r^{-2}$ (Fig. 2). Precisely what controls this cross-over remains uncertain. Geometric consideration based on the size and density of porter site on the cell have been explored as have the kinetics of porter handling times and energy costs (Box 1) but remain unresolved.

As a practical solution, we turn to observations. The available data are, however, very scattered (Fig. 2; see Table 1 for a summary of all parameters) and are in practise only useful to define the upper limit to the affinity. The data do confirm the theoretical prediction of an upper limit to encounter by diffusion limitation. They also indicate that the affinity of smaller cells (smaller than around $r_{\mathrm{D}}^* = 0.75$ µm) is limited by another process than diffusion limitation, which could be porter limitation. The conclusion is that we have a fully developed theoretical apparatus to understand the affinity of cells to dissolved organic matter, however, we need a better understanding of the specific processes related to molecule capture to fully relate affinity to fundamental processes.

Finally, the actual uptake is limited by the rate at which porters can transport the captured molecules across the cell membrane. This limitation is a surface process that scales with r^{-1} and the density of porters. As will be evident later, this limitation is unlikely to by relevant for diffusive uptake. It is therefore reasonable to describe diffusive uptake as in eq. (3).

Box 1: derivation of nutrient affinity

The diffusive flux to a partial absorbing sphere of radius r has a well known solution:

$$Q = 4\pi r D(N - N_0) \tag{6}$$

where D molecular diffusivity, and N and N_0 the nutrient concentration at distance and on the cell surface respectively. For a perfectly absorbing sphere $N_0 = 0$ and the flux becomes $Q = 4\pi r D N$. A real cell however is not perfectly absorbing but is covered by a finite number of uptake sites in an otherwise impervious cell wall. A classic result (Berg and Purcell, 1977) considers the cell surface covered by n porter sites each of radius s. If sites are small (specifically $s \ll r$), sparsely distributed, and perfectly absorbing, then the diffusive flux towards each site is $Q_s = 4sDN_0$. For n such sites then

$$Q = 4\pi r D(N - N_0) = 4nsDN_0 \qquad \Rightarrow N_0 = N\frac{\pi r}{\pi r + ns} \tag{7}$$

which leads to (Berg and Purcell, 1977)

$$Q = 4\pi r D N \frac{ns}{\pi r + ns}. \tag{8}$$

A correction accounts for potential interference of diffusive fluxes when porter sites become tightly packed (Zwanzig, 1990). Specifically, expressing the surface fraction of porters as $p = ns^2/(4r^2)$

$$N_0 = N\frac{\pi r(1-p)}{\pi r(1-p) + ns} \qquad \Rightarrow Q = 4\pi r D N \frac{ns}{\pi r(1-p) + ns}. \tag{9}$$

As $p \to 1$ (i.e. the entire cell surface becomes covered with perfectly absorbing porter sites) $N_0 \to 0$ and $Q \to 4\pi r D N$. While theoretically sound and widely built upon, these results are actually not particularly germane to the question of nutrient dynamics in plankton. In the first instance, for typical cell sizes and porter sizes, the correction (9) saturates extremely rapidly so a very low porter density is sufficient to achieve near maximum uptake flux (Jumars et al., 1993). This implies that limitation of the number of porter sites due to surface crowding is unlikely to be an issue. Secondly, it is not realistic that uptake sites are perfectly absorbing discs. While diffusion towards the sites is a fair representation, uptake requires active transport across the cell wall (Aksnes and Egge, 1991; Armstrong, 2008), a process that (1) occupies the uptake site for a finite amount of time and (2) is energetically costly, requiring about 1 mole of ATP per mole of nutrient transported.

2.2.2 Light harvesting; theory and data

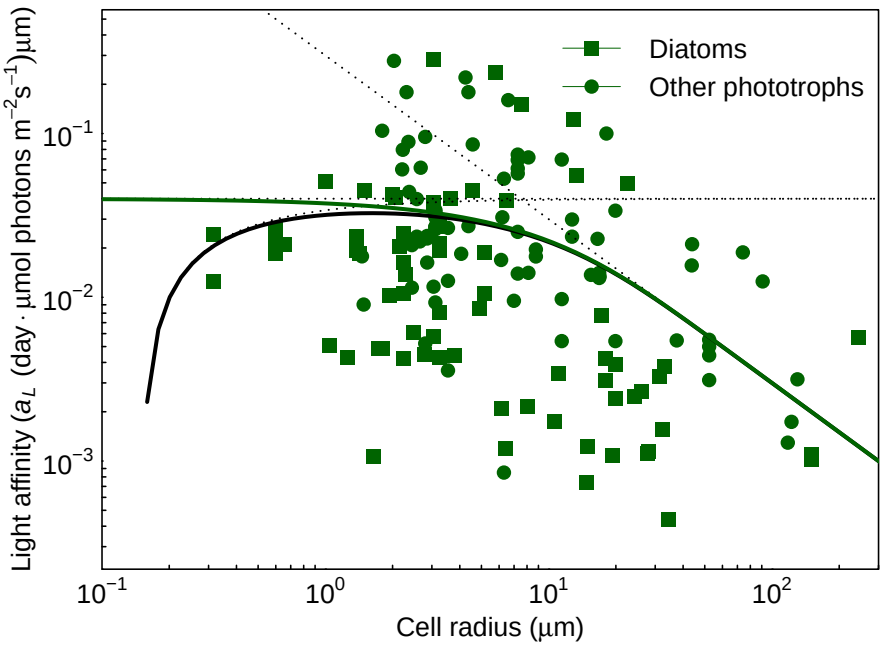

Figure 3: Light affinities of protists as a function of carbon mass compared to the first-principles formulae (13; thick black line and (12); green line). The three limiting factors: cells mass, cell surface, and cell wall are shown with dotted lines. The black line is the total affinity. Data from Edwards et al. (2015), corrected for day length.

Box 2: derivation of light affinity

The net absorption of light by a cell depends on the density and distribution of individual chromophores within the cell's cytoplasm. Assuming a spherical cell (radius r) with uniformly distributed chromophores with mean number density c (μm^{-3}), and each with an optical cross section a (μm^2), then the rate at which photons are absorbed is given by (Duyens, 1956; Kirk, 1975):

$$Q(r,\lambda) = \frac{\pi L}{2\lambda^2}\left[(1+2\lambda r)\exp(-2\lambda r) + (2\lambda^2 r^2 - 1)\right] \tag{10}$$

Here $\lambda = ac$ (μm^{-1}) is the light absorption coefficient within the cytoplasm, and L ($\mu\text{mol}\,\text{m}^{-2}\text{s}^{-1}$) is the light flux. This relationship, while exact for a sphere, is somewhat clumsy. A more accessible formulation, assumes a cylindrical cell with the same volume and cross-sectional area as the sphere. Under this geometry, the optical path through the cell is $4r/3$ and (Hansen and Visser, 2019)

$$Q(r,\lambda) = \pi L r^2\left(1 - \exp(-4\lambda r/3)\right) \tag{11}$$

Given that these formulae give very nearly identical results, and precise shape is always a confounding factor, we opt for the simpler. From the form of (11) it is clear that for large cells ($\lambda r \gg 1$), $Q \approx \pi r^2 L$ whereas for small cells ($\lambda r \ll 1$), $Q \approx 4/3\pi r^3 \lambda L$.

Writing the quantum yield y (g/(mol photon)), specific light affinity becomes $a_\text{L} = y(Q/L)/m$. We can also write $\lambda = \kappa_\text{L}\phi_\text{L}$ relating the cell's absorption coefficient to ϕ_L, the fraction of its carbon mass invested in light harvesting where κ_L the constant of proportionality. Observations indicate that $\lambda = 0.1$ μm^{-1}(Raven, 1984, 1997) when about half of the cell's mass is devoted to light harvesting, suggesting that $\kappa_\text{L} = 0.2$ μm^{-1}. It follows then that

$$a_\text{L} = \frac{3y}{4\rho}\frac{1}{r}\left(1 - \exp(-4\kappa_\text{L}\phi_\text{L} r/3)\right), \tag{12}$$

which is identical to (13) with parameters $(\alpha_\text{L}, r_\text{L}^*)$ corresponding to $(3y/(4\rho), 3/(4\lambda))$ respectively. Quantum yield estimates ranges from 0.12 to 0.6 g_C/(mol photon) (Kishino et al., 1986). Using $y = 0.16$ gC/(mol photon) suggests $\alpha_\text{L} = 0.30$ $(\text{d}\,\mu\text{mol}\,\text{m}^{-2}\text{s}^{-1})^{-1}\mu\text{m}$ and $r_\text{L}^* = 7.5$ μm.

Fig. 3 shows that there are cells with almost a factor 10 higher affinity that predicted by (12). The source of this variation is likely due to uncertainty in the quantum yield y, which depends on the type of pigment and the wavelength of the light (Kishino et al., 1986).

Light harvesting happens when a photon is captured by the light harvesting complex. The number of photons caught is proportional to the number of light harvesting complexes, which scales with the functional cell mass. The mass specific light affinity a_{L} is therefore independent of cell size for large cells but limited by functional mass as $1-\nu$ for smaller cells (2). However, light harvesting complexes shade one another and in larger cells only the complexes in the surface are effective for light harvesting (Morel and Bricaud, 1981). The affinity for light harvesting therefore transitions from being independent of size for small cells to being proportional to the surface for large cells (see Box 1):

$$a_{\mathrm{L}} = \alpha_{\mathrm{L}} r^{-1}(1-\exp(-r/r_{\mathrm{L}}^{*}))(1-\nu). \tag{13}$$

This formulation of affinity has asymptotic scaling of $a_{\mathrm{L}} \to \alpha_{\mathrm{L}}/r_{\mathrm{L}}^{*}$ for intermediate cells, $a_{\mathrm{L}} \to \alpha_{\mathrm{L}}/r$ for $r \gg r_{\mathrm{L}}^{*}$ and goes to zero for small cells (the factor $1-\nu$).

Previous analyses of light affinity has focused on fitting one power law and has consistently found a scaling close to the predicted surface law $\propto r^{-1}$ (Taguchi, 1976; Edwards et al., 2015). Reanalysing the available data clearly shows a transition from mass to surface scaling with a transition size around $r_{\mathrm{L}}^{*} \approx 8 \pm 3$ µm(Fig. 3) in accordance with the first-principles argument in Box 1. The divergence to zero for smaller cells is consistent with a lower limit of one chloroplast at cell volume of ≈ 1 µm^3 or $r \approx 0.5$ µm(Okie et al., 2016).

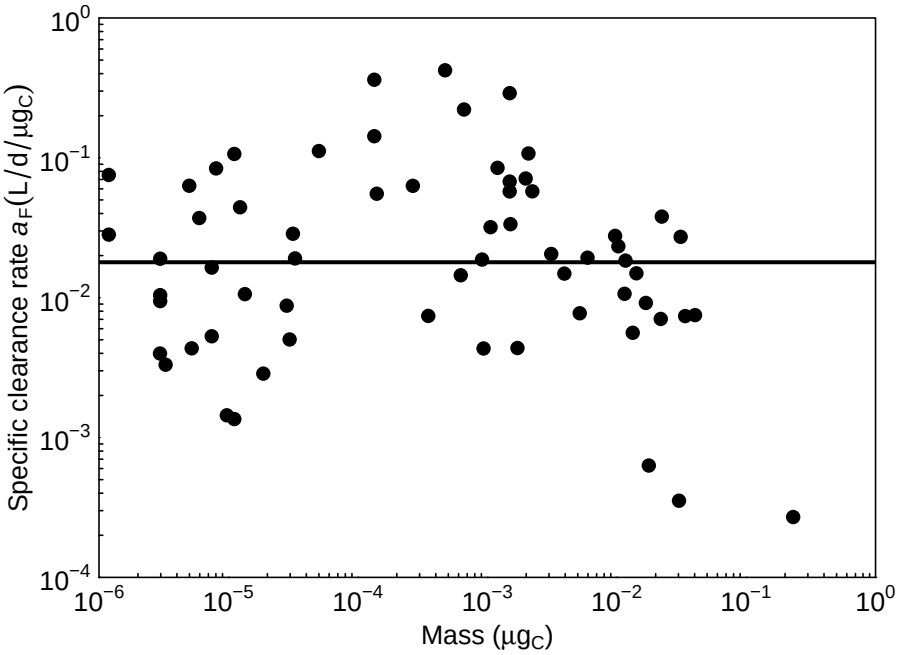

Figure 4: Specific clearance rate (a_{F}) as a function of carbon mass. Data of nanoflagellates, dinoflagellates, and ciliates from Kiørboe and Hirst (2014).

2.2.3 Phagotrophy

Box 3: Derivation of clearance rate

The specific clearance rate a_{F} (volume/time/cell mass) can be estimated from the work required to move the fluid that a cell filters. We assume that the work is approximately the same as pushing a sphere through the fluid, i.e., given by Stokes' law: $W = 6\pi\mu u^2 d$, where u is the velocity, d the cell diameter, and μ the dynamic viscosity of water. The power that the cell has available to filter water scales with the cell's mass $cm\rho_{\mathrm{e}}$, where c is the fraction of the cell's mass that can be used per time and ρ_{e} is the energy density of the cell. Equating the work needed and the power available gives the velocity as:

$$u = \sqrt{\frac{cm\rho_{\mathrm{e}}}{6\pi\mu d}}.$$

Assuming that the cell clears an area corresponding to its own cross section we get the specific clearance rate as the clearance area $\pi(d/2)^2$ multiplied by the velocity and divided by the mass:

$$a_{\mathrm{F}} = \sqrt{\frac{c\rho_{\mathrm{e}}}{4\mu\rho}},$$

using (1) to convert between diameter and mass. The specific clearance rate is constant (independent of cell size). With a dynamic viscosity of $\mu = 1$ g/(m s), energy density $\rho_{\mathrm{e}} = 40 \cdot 10^3 \mathrm{m}^2 g \mathrm{s}^{-2} \mathrm{g_C}^{-1}$ (Boudreau and Dickie, 1992), and that the fraction of body mass used for driving the flow is 0.1 day^{-1}gives $a_{\mathrm{F}} = 0.0073$ l/day/µg$_{\mathrm{C}}$, very close to the geometric average of 0.018 from data in Fig. 4.

Phagotrophy is the ingestion of food particles, typically smaller cells. Prey cells are encountered either by the predator moving through the fluid or with the predator creating a feeding current that brings prey towards it (Kiørboe, 2011). The clearance rate (the volume of fluid searched per time) can be derived from a combination of fluid mechanics and the metabolic energy available to a cell, which shows that the specific clearance rate is approximately independent of cell size (Box 3, Fig. 4). The rule of thumb is that a zooplankton filters roughly 1 million of its body volume per day. For the actual food consumption, we also need to consider the limitation imposed by assimilation over the food vacuole membrane, which scales with the surface of the vacuole $\propto r^2$. The uptake limitation depends on the amount of food available. It is therefore different from the uptake limitation that acts in the nutrient and light affinities. The effective uptake then becomes:

$$j_{\mathrm{F}} = \epsilon_{\mathrm{F}} c_{\mathrm{F}} r^{-1} \frac{a_{\mathrm{F}} F}{a_{\mathrm{F}} F + c_{\mathrm{F}}/r}. \tag{14}$$

This formulation has the limit $j_{\mathrm{F}} \to \epsilon_{\mathrm{F}} a_{\mathrm{F}} F$ for smaller cells and $j_{\mathrm{F}} \to \epsilon_{\mathrm{F}} c_{\mathrm{F}}/r$ for larger cells with the cross-over size between the two regimes being food-dependent: $r^*_{\mathrm{F}} = c_{\mathrm{F}}/(\alpha_{\mathrm{F}} F)$. We do not have any direct measurements of the limitation due to the uptake, however, we will use the measurements of maximum growth rate of larger cells to estimate this process as $c_{\mathrm{F}} \approx 30$ µgµm/day. It can be argued that the cell wall should lead to a similar reduction in phagotrophy as is done for phototrophy. However, phagotrophy is not relevant for the smallest cells because they have no suitable food, so including the effect of

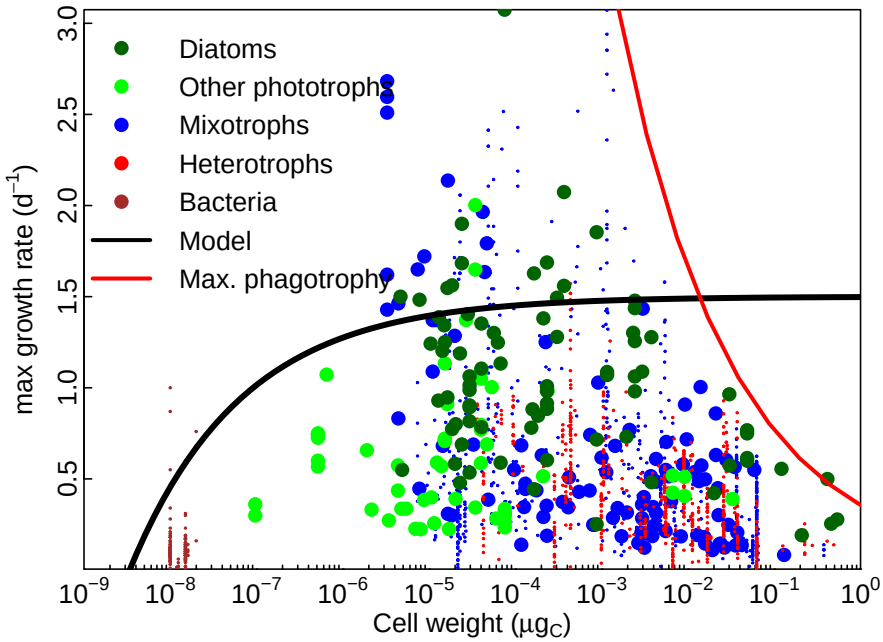

Figure 5: Maximum and observed growth rates (large and small symbols). Phototrophs from Edwards et al. (2015), mixotrophs (nano- and dinoflagellates and ciliates from Kiørboe and Hirst (2014) and "bacterivores" from Rose and Caron (2007)), heterotrophs ("herbivores" from Rose and Caron (2007)) and of bacteria (Kirchman, 2010). Rates are converted to 10 degrees with a $Q_{10} = 1.5$ for phototrophs and $Q_{10} = 2.8$ for mixo- and heterotrophs. The solid line is a (16) with $\alpha_{\max} = 1.5$ day^{-1}. The red line is the maximum assimilated phagotrophic uptake $\epsilon_{\mathrm{F}} c_{\mathrm{F}} r^2$.

cell walls for phagotrophy is irrelevant.

2.3 Passive losses across the membrane

Losses of dissolved organic carbon and nutrients by the cell is not well understood. Some losses are "income taxes" incurred during uptake, which is represented as a less than 100% efficiency of the uptakes. Other losses are simply passive exudation of small organic compounds across the membrane as a "property tax" *sensu* Bjørnsen (1988). The passive exudation can be assumed to scale with the surface area (Kiørboe, 2013) and, assuming a negligible external concentration, becomes:

$$j_{\mathrm{passive}} = c_{\mathrm{passive}} r^{-1}, \tag{15}$$

where $c_{\mathrm{passive}} = 3P$ where $P \approx 1$ µm/day is the permeability of a phytoplankton membrane (Bjørnsen, 1988). However, considering than only about 10% of the compounds are of sufficiently low molecular weight to escape through the membrane, c_{passive} should be reduced by a factor 10. Further, the smallest cells, which are those which are most affected by passive exudation losses, are bacteria with a different cell wall than the phytoplankton considered by Bjørnsen (1988). We therefore further reduce the permeability by a factor 10 and use $c_{\mathrm{passive}} \approx 0.03$ µm/day. Note that Braakman et al. (2017) argues for membrane permeability in excess of $\approx 10^6$ µm/day, which implies that the cell spends significant amounts of energy continuously re-uptaking lost nutrients.

2.4 Biosynthesis and basal metabolism

The maximum rate of biosynthesis is limited by the cell's investment in synthesis machinery, i.e., ribosomes. If we consider the number of ribosomes to be proportional to cell mass then the synthesis rate – the biomass synthesized per time and per cell mass – becomes independent of functional cell mass, i.e., $\propto 1 - \nu$ (a more detailed allocation can be made with optimization approaches (Shuter, 1979; Serra-Pompei et al., 2019, e.g.)). The maximum synthesis capacity j_{max} is assumed to be independent of mass and limited by the cell wall fraction (2):

$$j_{\mathrm{max}} = \alpha_{\mathrm{max}}(1 - \nu). \tag{16}$$

The division rate is further limited by the basal metabolism. The basal metabolism supports the functions needed to keep the cell alive but not the respiration associated with resource assimilation and biosynthesis. In this simple model we do not distinguish between basal metabolism and other respiration (but see Chakraborty et al. (2017, 2020)) and consider simply that all respiratory costs are a fraction of cell mass, and therefore that j_{R} is constant. For simplicity we write it proportional to the maximum synthesis capacity:

$$j_{\mathrm{R}} = \alpha_{\mathrm{R}}\alpha_{\mathrm{max}}. \tag{17}$$

with $\alpha_{\mathrm{R}} \approx 0.1$.

2.5 Temperature effects

Temperature effects are introduced by multiplying rates with a Q_{10} function: $Q_{10}^{(T-T_{\mathrm{ref}})/10}$ which gives the fractional increase in the rate when the temperature is increased 10 degrees from a reference temperature of $T_{\mathrm{ref}} = 10$ degrees. The Q_{10} factors are $Q_{10} = 1.5$ for diffusive uptakes, no temperature correction for light uptake and feeding , while there is a standard "metabolic" correction of $Q_{10} = 2$ on respiration, maximum phagotrophy, and maximum synthesis capacity (Serra-Pompei et al., 2019).

Table 1: Parameters for the cell-level processes (Section 2) and the size-based model (Section 4). "d" is the unit of time (days).

Parameter	Value	Reference
Cell size and density		
Carbon density	$\rho = 0.4 \cdot 10^{-6}$ µg$_\mathrm{C}$/µm^3	(a)
Membrane thickness	$\delta = 50$ nm	
C:N mass ratio	$\rho_{\mathrm{C:N}} = 5.68$ g$_\mathrm{C}$/g$_\mathrm{N}$	
Cell rate parameters		
Diffusive aff. coef.	$\alpha_\mathrm{D} = 0.972$ l·µm^2/d/µg$_\mathrm{C}$	Fig. 2, Box 1
Diffusive aff. cross-over	$r^*_\mathrm{D} = 0.75$ µm	Fig. 2, Box 1
Light aff. coef.	$\alpha_\mathrm{L} = 0.3$ (d·µmol m^{-2}s^{-1})$^{-1}$µm	Fig. 3, Box 2
Light aff. cross-over	$r^*_\mathrm{L} = 7.5$ µm	Fig. 3, Box 2
Light uptake eff.	$\epsilon_\mathrm{L} = 0.8$	
Clearance rate	$a_\mathrm{F} = 0.018$ l/d/µg$_\mathrm{C}$	Fig. 4, Box 3
Max. phagotrophy coef.	$c_\mathrm{F} = 30$ µm/d	Fig. 5
Assimilation efficiency	$\epsilon_\mathrm{F} = 0.8$	
Passive loss coef.	$c_\mathrm{passive} = 0.03$	See text
Max. synthesis coef.	$\alpha_\mathrm{max} = 1.5$ d^{-1}	Fig. 5
Basal metabolism coef.	$\alpha_\mathrm{R} = 0.1$	
Prey encounter		
Predator-prey mass ratio	$\beta = 500$	(b)
Predator-prey width	$\sigma = 1.3$	(b)
Community model parameters		
DOC remin. of feeding	$\gamma_\mathrm{F} = 0.1$	
DOC remin. of lysis	$\gamma_\mathrm{v} = 0.5$	
Lysis mortality coef.	$\mu_{\mathrm{v}0} = 0.004/\log(m^+/m^-)$	(c)
Size of HTL mort.	$m_\mathrm{htl} = 8.9 \cdot 10^{-5}$ µg$_\mathrm{C}$	(d)
HTL mortality coef.	$\mu_{\mathrm{htl}0} = 0.1$ d^{-1}	
Chemostat parameters		
Mixing rate	$d = 0.0001...1$ d^{-1}	
Deep nutrient conc.	$N_0 = 50$ µg$_\mathrm{N}$/l	
Productive layer	$M = 20$ m	

(a) Rough average of data on protists excl. protists in Menden-Deuer and Lessard (2000). (b) Rough average from Fig. 6.6 in Kiørboe (2008). (c) Inversely proportional to the log width of the computational cells, $\log(m^+/m^-)$. Adjusted to be smaller than the predation mortality. (d) A factor $\beta^{1.5}$ smaller than the largest size in the simulations (1 µg$_\mathrm{C}$).

3 Analysis of size-based processes

Just considering the rates of uptakes and losses of cells provides insights into the plankton community structure and dynamics. The size-based relations determine the extreme cell sizes: the smallest and the largest cells, and they determine the limiting resources, i.e., the levels of resources needed for subsistence, and the cell size which can survive on the lowest resource levels.

3.1 Smallest and largest cells

The smallest cell is limited by the cell wall (Raven, 1994). The absolute smallest size is when the cell wall uses the entire mass:

$$r_{\min} = \delta \approx 50\,\mathrm{nm} \approx 0.03\,\mu\mathrm{g}. \tag{18}$$

This is an extreme lower limit for a cell with plenty of resources and no losses. Considering that losses to respiration and passive losses (15) can not exceed the maximum synthesis rate (16): $j_{\max} > j_R + j_{\mathrm{passive}}$, gives a minimum size of:

$$r_{\min} = \frac{c_{\mathrm{passive}} + 3\alpha_{\max}\delta}{\alpha_{\max} - j_{\mathrm{R}}} \approx 0.2\,\mu\mathrm{m} \approx 0.16\,\mu\mathrm{g}. \tag{19}$$

This limitation is again an absolute limit because it does not consider mortality losses.

The largest cells are heterotrophs. They are limited by two processes: the rate at which oxygen diffuses into the cell (Chap. 1 in Fenchel, 1987; Payne et al., 2011) and the rate at which they can assimilate food through the walls of their feeding vacuoles (red line in Fig. 5). Here we only consider the limiting effects of food uptake. The maximum size $r_{\max}$ is when the maximum rate of assimilated consumption, $\epsilon_{\mathrm{F}} c_F / r$ (14) equals the metabolic costs j_{R}:

$$r_{\max} = \frac{j_{\mathrm{R}}}{\epsilon_{\mathrm{F}} c_{\mathrm{F}}} \approx 160\,\mu\mathrm{m} \approx 10\,\mu\mathrm{g}. \tag{20}$$

The upper limit fits with the prediction by Payne et al. (2011) of a maximum size ≈ 1 mm under present day oxygen conditions. Again, this is an extreme upper limit and the largest emerging cells are about a order of magnitude smaller. To overcome the upper limitation of size, organisms will have to become multicellular. The smallest adult copepods are on the order of 0.01 µg, which corresponds to the size where the feeding vacuole becomes limiting for growth (Fig. 5).

3.2 Limiting resources, R^*

The growth of plankton is limited by their ability to acquire and assimilate resources of nutrients, DOC, food from predation, and light. As dissolved resources are subject to competition by all cells, nutrients and DOC are exhausted to the lowest level that the most competitive groups can just survive on. This level is commonly referred to as the "R^*" value, *sensu* Tilman (1982). We can extend the concept to the concentration of food and light and food. Food is different than the dissolved resources because not all size groups

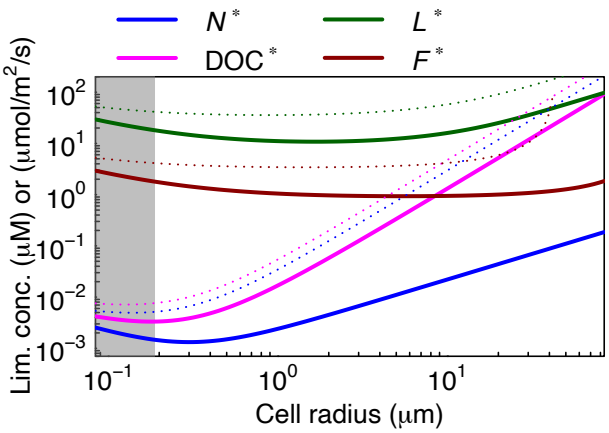

Figure 6: Minimum concentrations for survival solely on one resource (R^*). Shown with mortality $\mu = 0$ (solid lines) and $\mu = 0.4$ day^{-1} (dotted lines). Carbon sources (light and DOC) assume plenty of nutrients; N^* assume plenty of carbon; F^* is for a pure phagotroph. The grey area indicates the minimum viable size of a cell (19).

compete for all sizes of food due to size-based selection. Nevertheless, F^* indicates the minimum level of biomass of their prey. Finally, we can calculate the minimum level of light L^* where purely phototrophic plankton can survive. Plankton does not compete for light (except in extreme cases of biomass as seen in some fresh water environments; Klausmeier and Litchman (2001)), but the L^* indicates the minimum light level – and thus the maximum depth – where photosynthesis alone can support plankton growth.

We can find the limiting resources by calculating the resource level that just balances losses to exudation, respiration, and mortality, e.g., for light: $j_{\mathrm{L}}(L^*) = j_{\mathrm{passive}} + j_R + \mu$, where μ is mortality losses (see Table 2). N^* is calculated from the assumption that carbon is abundant so we can ignore respiration. Similarly, the calculation of L^* and DOC^* assumes abundant nutrients but no alternative carbon source (from DOC, light or food). F^* also assumes no other carbon source (no phototrophy or DOC).

The actual values of the limiting resources cannot be compared directly because they are in different units, however the limiting resources have a characteristic variation with cell size (Fig. 6). At smaller sizes the limiting process is passive losses; at larger sizes it is the decreasing affinity. The end result is that small cells are the most competitive for dissolved nutrients and DOC (at least when they are subjected to reasonable mortality losses). A very wide range of sizes can survive on the lowest light levels. Phototrophy therefore selects weakly for cell size, and the selection only enters because the cells also need nutrients, which select for small cells. The minimal food requirement F^* is almost independent of size and is around 1 μg_{C}/l. Again, cells do not compete much for food with cells of other sizes because of the size-selection for food.

Table 2: Limiting resource levels

$$N^*(r) = \frac{(c_{\text{passive}} + \mu r)(r^2 + r_{\text{D}}^2)}{r\alpha_{\text{D}}}$$

$$X^*_{\text{DOC}}(r) = \frac{(c_{\text{passive}} + (j_{\text{R}} + \mu)r)(r^2 + r_{\text{D}}^2)}{r\alpha_{\text{D}}}$$

$$L^*(r) = \frac{1}{1 - e^{-r/r_{\text{L}}}} \frac{c_{\text{passive}} + (j_{\text{R}} + \mu)r}{\alpha_{\text{L}}}$$

$$F^*(r) = \frac{c_{\text{F}}(c_{\text{passive}} + (j_{\text{R}} + \mu)r)}{c_{\text{F}}\epsilon_{\text{F}} - \alpha_{\text{F}} r(c_{\text{passive}} + (j_{\text{R}} + \mu)r-)}$$

4 Scaling from cells to the size spectrum

Box 4: Theoretical derivation of the size spectrum

If the cell is not limited by uptake over the feeding vacuole then the effective encounter rate is $j_{\mathrm{F}} = \epsilon_{\mathrm{F}} a_{\mathrm{F}} F$ (14). The encountered food F is found by inserting the ansatz $b(m) = \kappa m^{\lambda-1}$ in (27) to give $F(m) = \kappa m^{\lambda}\alpha$, where $\alpha = \sqrt{2\pi}\sigma\beta^{\lambda}e^{\lambda^2\sigma^2/2}$ is a factor that depends on the parameters of the size preference function 26. Following Andersen and Beyer (2006) we now assume that the encounter rate of food j_{F} is proportional to the metabolic needs j_{R} and independent of size. Then we can equate encountered food with metabolic needs:

$$\epsilon_{\mathrm{F}} a_{\mathrm{F}} \kappa m^{\lambda}\alpha \propto j_{\mathrm{R}}. \tag{21}$$

This equality is only true if the dependency on m disappears, i.e., if $\lambda = 0$. When $\lambda = 0$ the abundance distribution is $b(m) \propto m^{-1}$, corresponding to the Sheldon spectrum $\mathcal{B}$ (33) being constant (independent of cell size).

The level of the spectrum, κ, can be estimated by assuming that the entire flux of new nutrients dN_0 into the photic zone is taken up and used. The flux of potential new production is dN_0 which can support a new primary production of $dN_0\rho_{\mathrm{C:N}}$ ($\mathrm{g_C}$/day/liter). There are three sources of losses: higher trophic level predation, diffusion losses, and respiration. The losses to higher trophic levels are found by integrating over the range where the higher trophic level mortality acts, i.e., a factor β:

$$J_{\mathrm{HTLloss}} = \int_{m_{\mathrm{htl}}}^{\beta m_{\mathrm{htl}}} \kappa m^{-1}\mu_{\mathrm{htl}}\,\mathrm{d}m \tag{22}$$

$$= \kappa\mu_{\mathrm{htl}}\ln(\beta). \tag{23}$$

Diffusion and respiration losses are found by integrating over the entire size range:

$$J_{\mathrm{loss}} = \int_{m_{\mathrm{min}}}^{m_{\mathrm{max}}} \kappa m^{-1}(d + j_{\mathrm{R}})\,\mathrm{d}m = \kappa(d + j_{\mathrm{R}})\omega, \tag{24}$$

where the ranges of the integration are given by (19) and (20) and $\omega = \ln(m_{\mathrm{max}}/m_{\mathrm{min}}) \approx 25$. Equating the new production with losses and accounting for a fraction ϵ_{htl} of the higher trophic level losses being remineralized in the photic zone, gives:

$$\kappa = \frac{dN_0\rho_{\mathrm{C:N}}}{(1-\epsilon_{\mathrm{htl}})\mu_{\mathrm{htl}}\ln\beta + (d + j_{\mathrm{R}})\omega}, \tag{25}$$

The structure of the plankton community is described by its size distribution and the variation of trophic strategies (how cells acquire carbon) with size. Both aspect depends on the environment of light, nutrients, and temperature, but also of the available food $F(m)$. The concentration of food varies with cell size as it is determined by the abundance of smaller prey: the size spectrum. Nevertheless, it is possible to understand the broad-scale structure of the plankton community from the cell-levels rates combined with the assumption that the food concentration is constant.

4.1 Theoretical size spectrum

The size spectrum is the biomass distribution as a function of cell size $b(m)$. Being a distribution means that the spectrum has dimensions of biomass per cell mass and it is referred to as the "biomass size spectrum". It is convenient to also define the "Sheldon spectrum", which is the biomass in log-spaced size groups, which is proportional to $b(m)m$. This representation is useful because it is commonly observed that the Sheldon spectrum is independent of size (Sprules and Barth, 2016).

The flat Sheldon spectrum is commonly understood as emerging from predator-prey interactions (Sheldon et al., 1972; Andersen and Beyer, 2006). Among the lower trophic levels of the ocean, however, it is less clear that this explanation is valid because small cells mainly subsist on photosynthesis and recycled production from dissolved organic matter and less on predation on smaller particles. Keeping this caveat in mind, we will nevertheless explain the scaling of the community size spectrum only from considerations of predator-prey interactions and later show that the predictions fit surprisingly well with dynamical simulations.

Predator-prey interactions are described by bigger cells predating on smaller cells. The size preference for predation is described by a log-normal size selection function (Fig. 1):

$$\phi(m, m_{\mathrm{prey}}) = \exp\left[-\frac{\ln^2(m/(\beta m_{\mathrm{prey}}))}{2\sigma^2}\right], \tag{26}$$

where m_{prey} is prey size, β the preferred predator:prey mass ratio and σ the width of the preference function. The available food is found by integrating across all size groups:

$$F(m) = \int \phi(m, m_{\mathrm{prey}}) b(m_{\mathrm{prey}})\, \mathrm{d}m_{\mathrm{prey}}, \tag{27}$$

where $b(m)$ is the biomass size spectrum. From this description we can derive the size spectrum as (Box 4):

$$b(m) = \kappa m^{-1}, \quad \text{with} \quad \kappa = \frac{dN_0 \rho_{\mathrm{C:N}}}{(1-\epsilon_{\mathrm{htl}})\mu_{\mathrm{htl}} \ln\beta + (d + j_{\mathrm{R}})\omega}. \tag{28}$$

The spectrum scales with mass as m^{-1}, which means that the Sheldon spectrum $\propto b(m)m$ is constant. The height of the spectrum (the coefficient κ) is a novel result. The height depends on the mixing rate d, the concentration of nutrients being mixed up from the deep N_0, the mortality imposed by higher trophic levels μ_{htl}, and the length of the size spectrum $\omega = \ln(m_{\mathrm{max}}/m_{\mathrm{min}})$. The main controlling parameter is the mixing rate. The height of the spectrum increases with mixing but saturates at high mixing rates ($d \gg \mu_{\mathrm{htl}} \ln\beta/\omega$). At very high mixing rates the production will be limited by the synthesis capacity of the cell, which is not accounted for here, however, that is probably a rare occurrence in nature.

4.2 Trophic structure

The other dimension of community structure is the trophic strategies, i.e., how cells acquire resources: by osmotrophy (diffusive uptake of DOC), phototrophy, or by phagotrophy.

Table 3: Processes and equations to calculate the division rate g of a cell. All rates are in units of g_C/g_C per time.

Encounter and synthesis:		
Available carbon	$j_{\mathrm{C.net}} = j_{\mathrm{DOC}} + j_{\mathrm{L}} + j_{\mathrm{F}} - j_{\mathrm{R}} - j_{\mathrm{passive}}$	(M1)
Available nutrients	$j_{\mathrm{N.net}} = j_{\mathrm{N}} + j_{\mathrm{F}} - j_{\mathrm{passive}}$	(M2)
Leibig's law	$j_{\mathrm{net}} = \min\{j_{\mathrm{C.net}},\, j_{\mathrm{N.net}}\}$	(M3).
Synthesis	$g = j_{\max}\frac{j_{\mathrm{net}}}{j_{\mathrm{net}}+j_{\max}}$.	(M4)
Down-regulation of uptakes		
Feeding	$\tilde{j}_{\mathrm{F}} = \max\{0,\, j_{\mathrm{F}} - (j_{\mathrm{net}} - g)\}$	(M5)
Photoharvesting	$\tilde{j}_{\mathrm{L}} = j_{\mathrm{L}} - \max\{0, \min\{(j_{\mathrm{C.net}} - (j_{\mathrm{F}} - \tilde{j}_{\mathrm{F}}) - g),\, j_L\}\}$	(M6)
DOC uptake	$j_{\mathrm{DOC}} = g - \tilde{j}_{\mathrm{F}} - \tilde{j}_{\mathrm{L}}$	(M7)
Mortalities:		
Predation:	$\mu_{\mathrm{p}}(m_j) = \sum_i \frac{\tilde{j}_{\mathrm{F}.i}}{\epsilon_{\mathrm{F}}}\frac{\Phi_{ij}}{F_i}B_i$	(M7)
Viral lysis:	$\mu_{\mathrm{v}.i} = \mu_{\mathrm{v}0}B_i$	(M8)
Higher trophic levels:	$\mu_{\mathrm{htl}}(m) = \begin{cases} \mu_{\mathrm{htl}0}\phi(m,m) & \text{for } m < m_{\mathrm{htl}} \\ \mu_{\mathrm{htl}0} & \text{for } m \geq m_{\mathrm{htl}} \end{cases}$	(M9)

All fluxes are calculated according to the relations in Section 2. Available food is $F_i = \sum_j \Phi_{ij}B_j$ where the effective preference between size groups Φ_{ij} is found by integration across the width of the size groups (Appendix A). The tildes above the uptakes of light and food indicates down-regulation in eqs. (M5-6). (M1-2): Uptakes are given by (3) combined with affinities for nutrients and DOC (5), light (13) and food (14 and 27). (M3): a standard functional type II response aka. "Monod" function. (M7): The predation mortality exerted by unicellular plankton can be calculated as the ratio between the amount of food eaten by all predators from size group j and biomass at size group j. The amount eaten is: $E_j = \sum_i(\tilde{j}_{\mathrm{F}.i}/\epsilon_{\mathrm{F}})B_i\phi(m_i,\, m_j)B_j/F_i$. Moving B_j outside the sum to calculate predation mortality as $\mu_{\mathrm{p}.j} = E_j/B_j$ gives M7.

The dominant strategy is determined by which of the three fluxes j_{DOC}, j_{L} and J_{F} is the largest. Fig. 7a shows the fluxes of DOC, carbon from phototrophy, nutrients, and food in an environment specified by concentrations of DOC, N and food (specified by the level of the size spectrum κ), and by light. Typically, very small cells are osmotrophs, somewhat larger cells are light-limited phototrophs, medium-sized cells are nutrient limited and larger cells are mixotrophs or heterotrophs. The sizes where the dominant strategies transition varies though: less nutrients or more available food favours mixotrophic and heterotrophic strategies, while more DOC favours osmotrophy.

4.3 Dynamic size-based model

Further insight requires numerical simulations. Here we simulate the entire unicellular plankton community by embedding the model of cell resource uptake and metabolism in a simple ecosystem model. Cells are divided into size group with each group i representing the biomass B_i within a range of cells with the geometric mean mass m_i. For simplicity

cells have constant C:N mass ratio $\rho_{\mathrm{C:N}} = 5.68$, but the model can be extended to dynamic stoichiometry (Ho et al., 2020; Ward et al., 2018). The rate of change of biomass in a size group is:

$$\frac{1}{B_i}\frac{\mathrm{d}B_i}{\mathrm{d}t} = g(m_i) - \mu(m_i), \tag{29}$$

where $g(m)$ is the division rate and $\mu(m)$ is the total morality. The division rate is determined by resource encounter and synthesis (Table 3, eq. M4).

Mortality have three contributions: predation by unicellular plankton μ_{p} through the process of big cells eating smaller cells (M7), viral lysis μ_2 (M8), and predation by higher trophic levels μ_{htl} (M9). Viral mortality is modelled by a quadratic loss term by assuming that viral mortality is proportional to biomass. Mortality by higher trophic levels acts on the largest size groups. We use a selection function consisting of combination of the logarithmic size selection function in (26) and a constant level.

Nutrients and DOC are updated with the uptakes and losses from the cell-level processes:

$$\frac{\mathrm{d}N}{\mathrm{d}t} = \frac{1}{\rho_{\mathrm{C:N}}}\sum_i \left(\underbrace{-j_{\mathrm{N}.i}}_{\text{Uptake}} + \underbrace{j_{\mathrm{passive}.i}}_{\text{Exudation}} + \underbrace{\max\{0, j_{\mathrm{N.net}.i} - g_i\}}_{\text{Surplus}} + \underbrace{\frac{1-\epsilon_{\mathrm{F}}}{\epsilon_{\mathrm{F}}}\tilde{j}_{\mathrm{F}.i}}_{\text{Feeding losses}} + \underbrace{\mu_{\mathrm{v0}}B_i}_{\text{Lysis}} \right) B_i \tag{30}$$

$$\frac{\mathrm{dDOC}}{\mathrm{d}t} = \sum_i \left(-\underbrace{j_{\mathrm{DOC}.i}}_{\text{Uptake}} + \underbrace{j_{\mathrm{passive}.i}}_{\text{Exudation}} + \underbrace{\frac{1-\epsilon_{\mathrm{L}}}{\epsilon_{\mathrm{L}}}\tilde{j}_{\mathrm{L}}}_{\text{Photoharvesting}} + \underbrace{\gamma_{\mathrm{F}}\frac{1-\epsilon_{\mathrm{F}}}{\epsilon_{\mathrm{F}}}j_{\mathrm{F}.i}}_{\text{Feeding losses}} + \underbrace{\gamma_{\mathrm{v}}\mu_{\mathrm{v0}}B_i}_{\text{Lysis}} \right) B_i. \tag{31}$$

Generation of N happens through assimilation losses, passive exudation and remineralised virulysis. Generation of labile DOC happens through passive exudation, assimilation losses from light harvesting and phagotrophy, and from remineralized viral lysis. We assume that all nutrient losses from viral lysis are made available over short time scales (Carlson, 2002), but only a fraction γ_{v} of carbon losses are labile. All the losses to higher trophic levels are eventually converted to particulate organic matter (which is not explicitly resolved here) so there is no remineralization of those losses.

Table 4: Box 4: definition of the Sheldon size spectrum

The structure of the plankton community is represented by the biomasses in the size groups B_i. This representation has the disadvantage that the level of the biomasses depend on the size-range of each group: broader (fewer) size-groups leads to higher average biomass level and *vice versa*. To avoid this dependency size distributions are often shown as "normalized size spectra" (Sprules and Barth, 2016), by divided the biomass with the size range of the group: $b(m_i) = B_i/(m_i^+ - m_i^-)$, where m_i^+ and m_i^- are the upper and lower sizes in the size group. If we assume a scaling biomass spectrum, $b(m) = \kappa m^{\lambda-1}$ then the relation between the normalized biomass spectrum and the binned size groups is:

$$B_i = \int_{m_i^-}^{m_i^+} b(m)\,\mathrm{d}m = \kappa \log(m_i^+/m_i^-) \tag{32}$$

if $\lambda = 0$. If size groups are evenly distributed on a log scale then m_i^+/m_i^- is constant (independent of mass) and the biomasses in each groups are roughly the same. To avoid that results depends on the binning of the size groups we here define the "Sheldon" spectrum as:

$$\mathcal{B}(m) = B_i/\log(m_i^+/m_i^-). \tag{33}$$

The system of coupled ordinary differential equations (29-31) is implemented in three model systems: a chemostat, a water-column and a global simulation. The chemostat simulates the upper photic zone of the ocean (Evans and Parslow, 1985). The upper layer is mixed with a deep layer with concentration $N_0 = 150$ μg_N of dissolved nitrate and zero concentrations of labile DOC and biomass. The water column and global simulations use a transport matrix formulation (Khatiwala et al., 2005; Khatiwala, 2007) with monthly transport matrices from the MIT global circulation model with a 1 degree resolution (Stammer et al., 2004). The system of ODEs can be integrated with standard ODE solvers; for the water column and global simulations we use an Euler solver with time steps of 0.1 day.

Chemostat simulations in eutrophic situations with a high mixing rate show an extended flat Sheldon spectrum occupying the full size range (Fig. 8). The level of the size spectrum fits with the theoretical prediction (25). Phototrophic cells span a wide size range and due to the high influx of nutrients they are light limited and not nutrient limited. Microplankton and partly nanoplankton have a significant influx of carbon and nutrients from phagotrophy. Only the largest cells are fully heterotrophic in the sense that they leak surplus nutrients.

Under oligotrophic situations with a low mixing rate the spectrum is still flat, but the

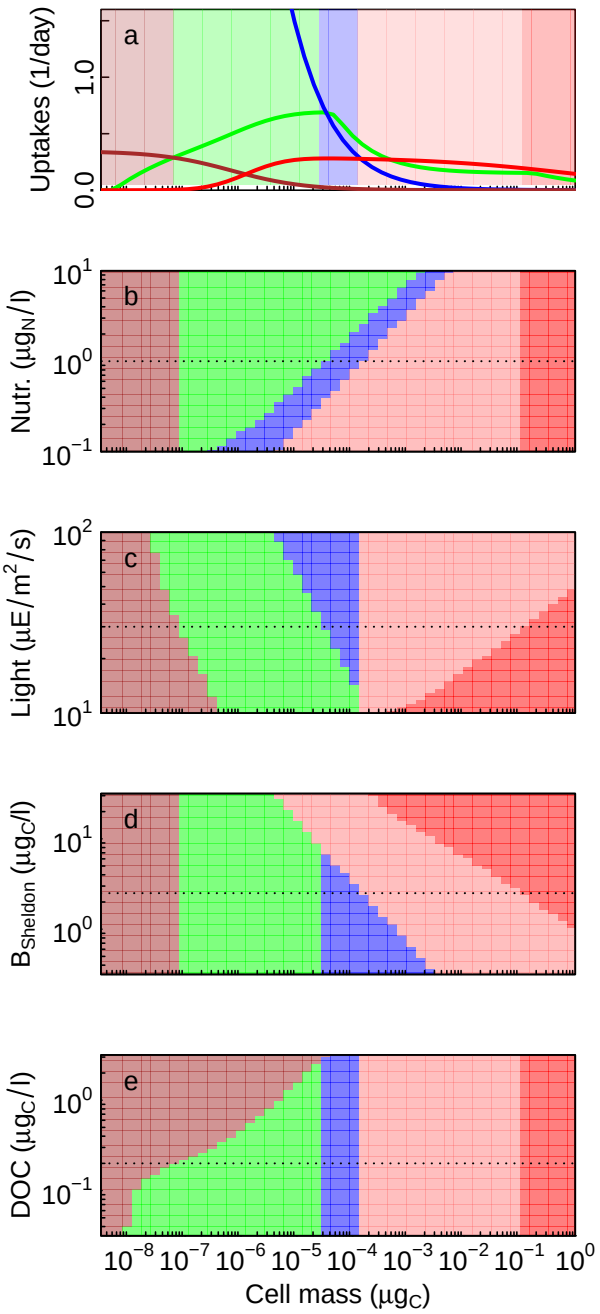

Figure 7: The trophic strategies of unicellular plankton under different environmental conditions. a) The gains from light (green), nutrients (blue), food (red), and DOC (brown), and phagotrophy (red). The dominant trophic strategy is shown by shading: heterotrophy, when surplus nutrient is leaked (red); mixotrophy when the carbon gain from phagotrophy surpass the potential gain from phototrophy (light red); nutrient limited phototrophy when the potential gain from light surpass the nutrient uptake (blue); light limited phototrophy when nutrient uptake surpass carbon uptake (green); osmotrophy when carbon from DOC surpass carbon from light harvesting (brown). b-e) Variations in the dominant trophic strategy with changes in nutrients, light, biomass and DOC around the conditions in panel (a) are indicated with a dotted line in each panel.

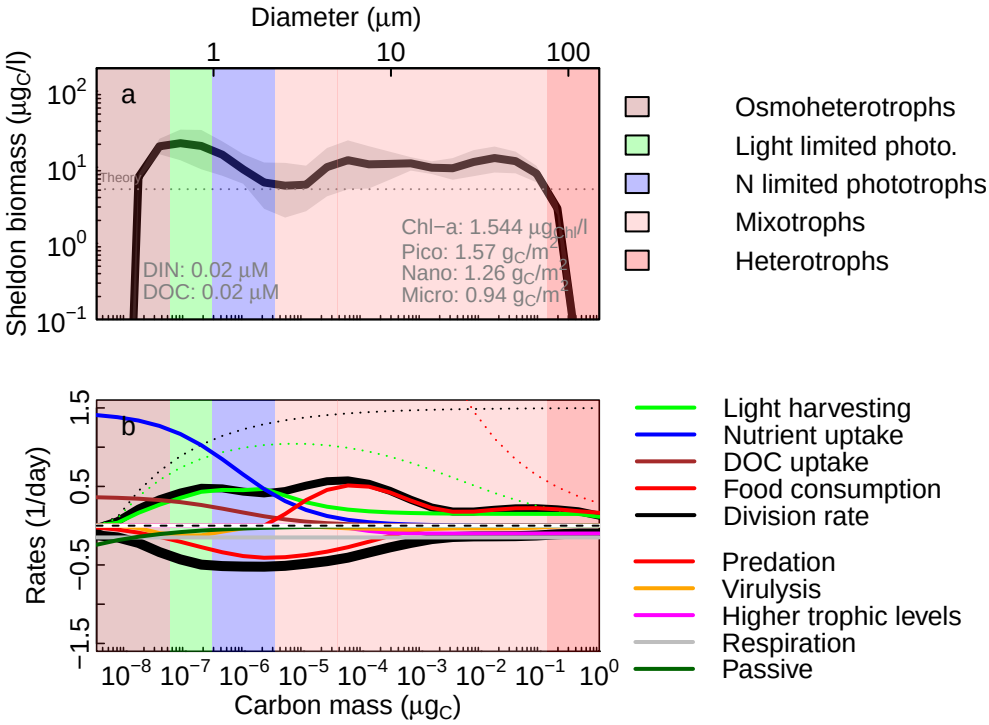

Figure 8: Results of simulations of the chemostat model for eutrophic conditions with high mixing. Top panel shows the Sheldon size spectrum (Box 4). The background colours indicate the trophic strategy (see Fig. 7). The lower panel shows rates of uptakes and losses in biomass specific units (day^{-1}). The dotted lines show maximum possible uptakes or growth rates. Parameters: Light $L = 40$ μE/m^2/s, mixing rate $d = 0.1$ m/day, and higher trophic level mortality $\mu_{\mathrm{htl}} = 0.1$ day^{-1}.

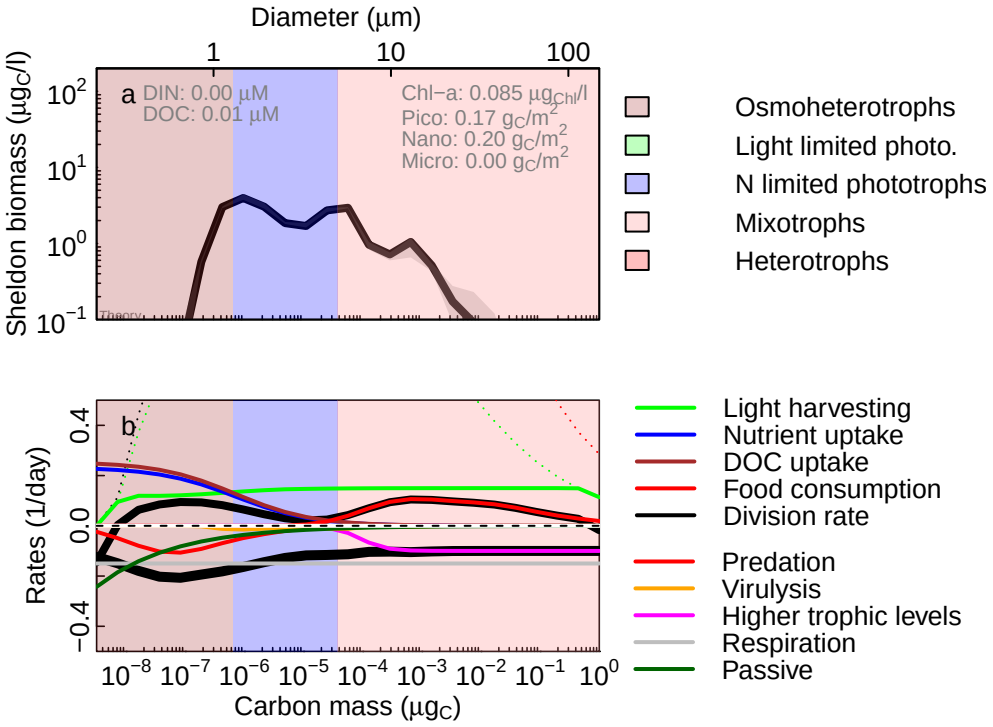

Figure 9: Results of simulations for an oligotrophic situation with low diffusivity of nutrients; see Fig. 8 for explanation (note different y-axis on panel b). Mixing rate $d = 0.001$ 1/day.

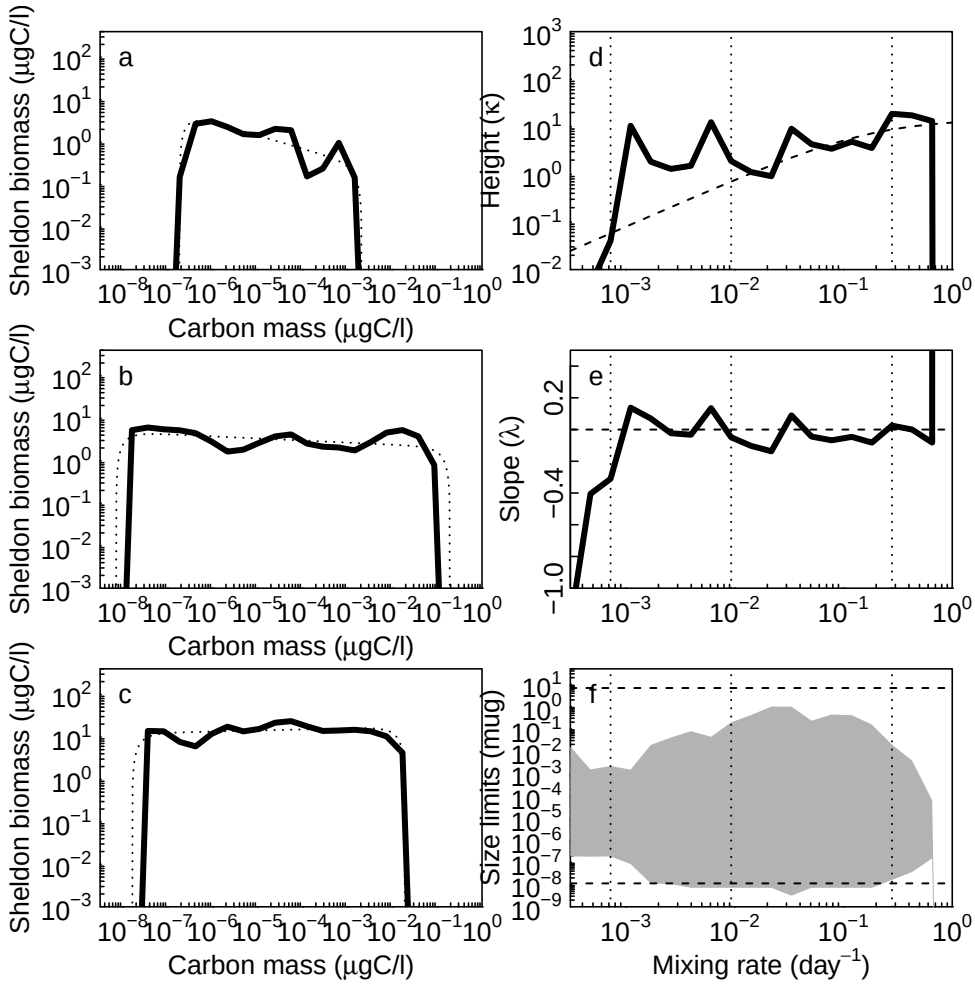

Figure 10: Size spectra from the chemostat with varying mixing rates under high light. Panels a-c: size spectra fitted to a power-law (28) truncated at high and low sizes (dotted). Panels d-f: results of the fits for height (κ), exponent (λ) and upper and lower size limits. The dashed lines are the theoretical predictions of κ from (25), exponent λ from (28), and min and max sizes from (19 and (20). The vertical dotted lines in panels d-f show the three mixing rates used to calculate panels a-c. $L = 100$ μE/m^2/s.

Table 5: Ecosystem biomass and functions. M is the thickness of the mixed layer, here set to 20 m.

Function	Formula	Value Olig.	Value Eut.	
Biomasses				
Biomass	$B_{\text{total}} = M \sum_i B_i$	0.38	3.8	g_C/m^2
Chlorophyl[(1)]	$B_{\text{Chl}} = M \sum_i \tilde{j}_{\text{L}.i} B_i / L$	0.085	1.5	$\mu g_{\text{Chl}}/l$
Production				
Gross PP	$P_{\text{gross}} = M \sum_i \tilde{j}_{\text{L}.i} B_i / \epsilon_{\text{L}}$	20	360	$g_C/m^2/yr$
Net PP	$P_{\text{net}} = M \sum_i \max\{0, \tilde{j}_{\text{L}.i} - j_{\text{R}.i}\} B_i$	0	150	$g_C/m^2/yr$
Net bact. prod.	$P_{\text{bact}} = M \sum_i \max\{0, j_{\text{DOC}.i} - j_{\text{R}.i}\} B_i$	0.12	66	$g_C/m^2/yr$
New prod.	$P_{\text{new}} = Md(N_0 - N)\rho_{\text{C:N}}$	2.1	210	$g_C/m^2/yr$
Prod. of HTLs	$P_{\text{htl}} = M \sum_i \mu_{\text{htl}.i} B_i$	2.5	60	$g_C/m^2/yr$
Efficiencies				
Eff. of PP	$\epsilon_{\text{PP}} = P_{\text{net}}/P_{\text{gross}}$	0.0	0.43	
Eff. of bact.	$\epsilon_{\text{bact}} = P_{\text{bact}}/P_{\text{net}}$	-	0.42	
Eff. of HTL	$\epsilon_{\text{htl}} = P_{\text{htl}}/P_{\text{net}}$	-	0.43	

[(1)] Mass of Chl per carbon mass is approximately proportional to the down-regulated mass-specific light affinity $\tilde{j}_{\text{L}.i}/L$. (Edwards et al., 2015).

realized size range is smaller in both ends of the spectrum. Therefore the level is also higher than predicted, because the prediction was only valid for a full range spectrum. Under oligotrophic situations the phototrophs are fully nutrient limited. It is surprising that very small cells are absent in oligotrophic conditions, because they are expected to dominate. This is because of the rising N^* values of small cells due to the limitation imposed by the cell wall (Fig. 6).

Simulating across mixing rates shows generally flat Sheldon size spectra (Fig. 10). The spectrum exponent (panel e) is roughly zero and the size spectrum level (κ) follows the prediction from (25) (panel d). Deviations occur for very small mixing rates where the spectrum becomes truncated (panel f) with a steep (negative) size spectrum and for very high mixing rates where the production is limited by the maximum synthesis rate, which is not represented in the simple arguments above. Overall it is clear that the overall exponent is unaffected by the environmental conditions, only the height and the extent of the spectrum are affected.

5 Ecosystem functions

The size distribution combined with the cell-level characteristics allows the calculation of ecosystem functions. Ecosystem functions can be divided into biomasses, production, and efficiencies. Because size-based models consider cells with multiple trophic strategies, calculating the functions are somewhat different than for ordinary functional group type of

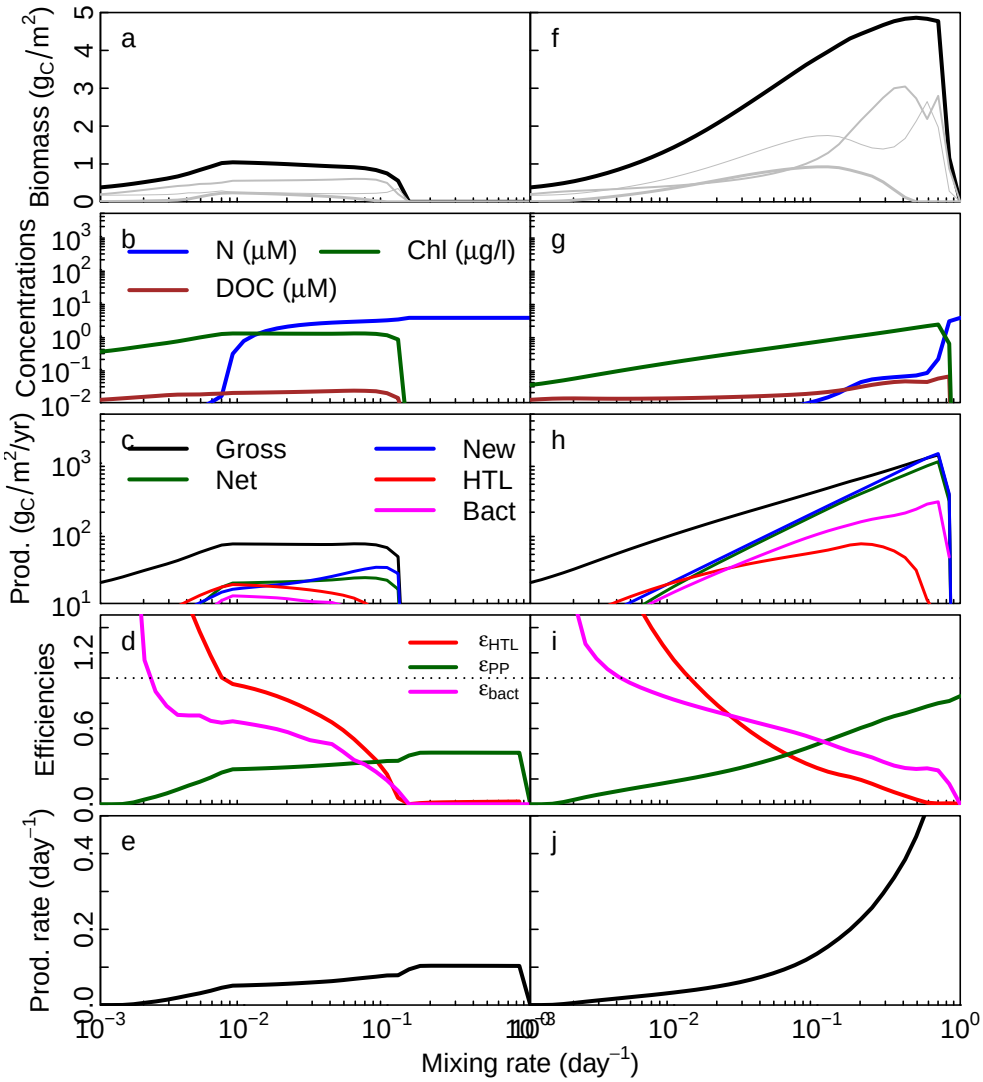

Figure 11: Ecosystem biomass and functions at low and high light ($L = 10$ and 100 μmol $m^{-2}s^{-1}$). In the top row the gray lines show pico-, nano-, and microplankton. The last row shows the production rate as the net primary production divided by biomass.

models (see Table 5). In the chemostat model the integration over the water column comes about simply by multiplying with the thickness of the productive layer $M \approx 20$ m.

Gross primary production is the total amount of carbon fixed :

$$P_{\mathrm{gross}} = M \sum_i j_{\mathrm{L}.i} B_i / \epsilon_{\mathrm{L}}. \tag{34}$$

The net production is usually considered as the carbon that is available for biomass production, i.e., the gross primary production minus the exudation losses and respiration. That definition, however, only works for purely phototrophic plankton. Here, plankton are mixotrophs and just applying the simple algorithm outlined above results in heterotrophs contributing negatively to primary production because they fix negligible amounts of carbon. To compensate, we consider only the groups where net fixation (fixation minus respiration) is positive. This procedure assumes that carbon from photosynthesis is prioritized for respiration over other carbon sources (DOC or feeding). Bacterial production is net production based on DOC uptake. It faces a similar problem as the net primary production, and again we only consider positive net contributions. For the chemostat model we can also calculate the new production as the amount of nutrient that diffuses up into the photic zone to fuel primary production. Finally, we can calculate the production to higher trophic levels as the losses to higher trophic level mortality.

Efficiencies are dimensionless numbers between 0 and 1. They are calculated as the ratio between a production and the net primary production.

Chemostat simulations show that total biomass is roughly proportional to the mixing rate d (25) until it becomes limited by light, around $d = 0.2$ day^{-1}in low light conditions (Fig. 11 a+f). The total Chl-concentration varies between 0.01 to 1 µgChl/l (panels b+g), which is in line with outputs of GCM simulations (Van Oostende et al., 2018). When production becomes light limited the nutrient level increases because plankton production cannot fix all the available nutrients (at mixing rates of 0.01 and 0.1 day^{-1} in low and high light respectively). The increases in biomass is reflected in the productions, which also increase roughly proportional to the biomass (panels c+h). However, the relative magnitude of the different productions changes with mixing rate, as reflected in the efficiencies (panels d+i). The production efficiency generally increases with the mixing rate. Surprisingly, the higher trophic level production can become larger than net primary production resulting in $\varepsilon_{\mathrm{htl}} > 1$. This occurs in oligotrophic situations where a high gross primary production fuels a high DOC production from exudation. That DOC also fuels plankton production, which eventually manifests itself in high net production to higher trophic levels. The gross efficiency of higher trophic level production ($P_{\mathrm{htl}}/P_{\mathrm{gross}}$ will always be < 1.

5.1 DOC and bacteria production

A difficult aspect of the ecosystem model is to parameterize the production and uptake of dissolved organic matter (DOC). Part of the difficulty stems from our incomplete knowledge of DOC: how much is labile and how much is not? And further: what are the sources of DOC: how much DOC is produced by incomplete assimilation and how much by passive exudation – or between "income" and "property" taxes (Bjørnsen, 1988)? In the ecosystem model DOC represents the labile DOC that can be immediately taken up and used.

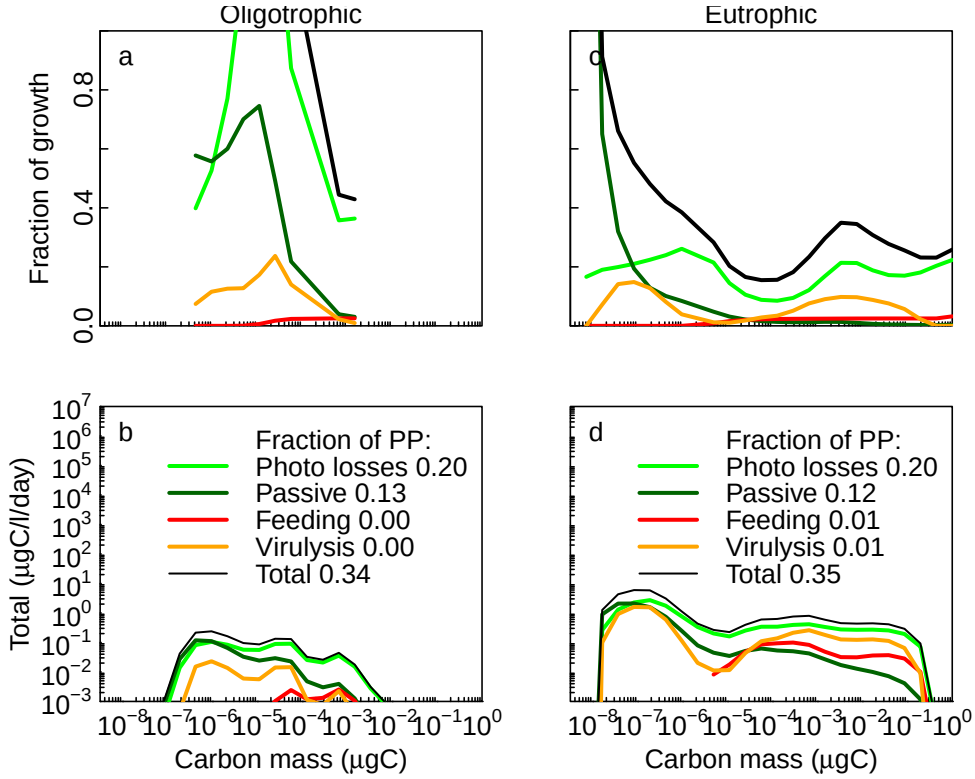

Figure 12: Losses to DOC as a function of cell size for oligotrophic conditions (Fig. 4.3) and eutrophic conditions (Fig. 8). Top row: losses as fraction of cell growth rate. Bottom row: total losses with fractions of gross primary production given in the legend.

Labile DOC is produced by incomplete assimilation of photoharvesting (ϵ_{L}), from passive exudation (j_{passive}), from assimilation losses due to feeding (ϵ_{F}), and from virulysis (j_{v}).

DOC release in pelagic ecosystem models are often described as a simple fraction of primary production (Thornton, 2014), though some include size-based passive exudation (Kriest and Oschlies, 2007) using Bjørnsen (1988)'s model, or a more complex division between labile and non-labile pools (Anderson and Williams, 1998; Flynn et al., 2008). The size-based model represents all processes: passive size-based exudation, exudation due to uptake, incomplete feeding, and virulysis, but does not distinguish between labile and refractory DOC.

All the incompletely assimilated carbon from photoharvesting is assumed to be available as DOC. The assimilation fraction is commonly set between 2-10%; following Anderson and Williams (1998) we use 20% ($\epsilon_{\mathrm{L}} = 0.8$) to have sufficient DOC available.

Passive losses are discussed in section "Passive losses across the membrane"; we as-

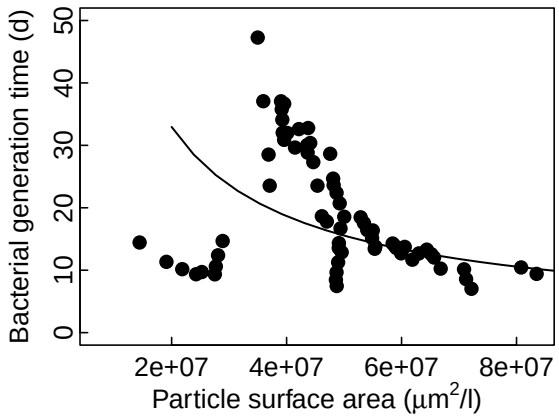

Figure 13: Bacterial productivity as a function of the total surface area of plankton in the size range ESD = 5 to 60 μmThe bacterial productivity is calculated as the flux of DOC uptake (j_{DOC}) minus losses to passive exudation and respiration: $\max\{0,\, j_{\mathrm{DOC}} - j_{\mathrm{passive}} - j_{\mathrm{R}}\}$. The generation time is 1 divided by the average of all bacterial productivities larger than 0. The lines shows a fit to a power law with fixed exponent -0.82. The mixing rate ranges between 0.001 and 0.1 $\mathrm{d}^{-1}$and light is from 10 to 60 μE/m^2/s.

sume that all passive losses are labile. Feeding losses from phagotrophy are set to 20% ($\epsilon_{\mathrm{F}} = 0.8$). However, not all feeding losses may be available, as mostly non-digestible material will be exuded; Anderson and Williams (1998) send only 10% of feeding losses back to DOC so we set the available fraction at $\gamma_{\mathrm{F}} = 0.1$. There is disagreement about the fraction of lysed cells that is available as labile DOC. Carlson (2002) find that the majority of the dissolved organic matter released from bacterial lysis is available, while (Anderson and Williams, 1998) only assume that 3.4% is available as labile DOC. We assume that half is available; $\gamma_{\mathrm{v}} = 0.5$. Feeding by higher trophic levels could also lead to DOC production. We assume that most sloppy feeding by higher trophic levels lead to particulate organic matter, which is not represented here, so $\gamma_{\mathrm{htl}} = 0$.

The model gives total DOC losses around 30 % (Fig. 12c+d), which is within the expected range. Overall we expect the average losses to DOC from passive exudation and assimilation losses from feeding to be 10-30 % of their production (growth rate) (Kiørboe, 1993; Carlson, 2002). This is within the range simulated by the model Fig. 12a+b. Smaller cells have much higher passive losses, which is essentially the process that determines the lower cell size.

The amount of primary production available for DOC should vary between 2-40%; highest in oligotrophic waters (Teira et al., 2001). In productive regions the main source of DOC is passive exudation while in unproductive it is assimilation losses from feeding (Teira et al., 2001). The observed fraction of primary production exuded is 2-40 % (Teira

et al., 2001; López-Sandoval et al., 2013); highest in oligotrophic regions. The model have a total losses in the same range (Fig. 12c+d legend). An important source in eutrophic waters is viral lysis while in oligotrophic waters the main source is photoharvesting.

Regarding the size-scaling of DOC losses the evidence is conflicted. Kiørboe et al. (1990) sees strong evidence of size-scaling of passive exudation, Teira et al. (2001) sees some indirect evidence, while Maranón et al. (2004) did not see any evidence (but notes that nutrient limitation may be a confounding factor). The diverging evidence reflects the difficulty in distinguishing between different sources of DOC and that studies focus on different size-ranges of cells. For example, López-Sandoval et al. (2013) notes that there is no overall size-scaling of DOC exudation among the plankton, which may be due to different processes dominating among small cells (passive exudation) and large cells (assimilation losses). The modelled total amount of DOC losses is roughly independent of size (Fig. 12b+c), though with higher passive losses for small cells. Among smaller cells the main source of losses are a combination of passive exudation, photosynthesis losses, and virulysis. Among larger cells feeding assimilation losses are a potential important term, which is, however, limited by the assumption that only a small fraction of feeding losses are labile ($\gamma_{\mathrm{F}} = 0.1$).

The only quantitative evidence on the size-relation between bacterial production and cell size is that the bacterial generation time is inversely correlated with the total surface area of plankton cells with a power-law exponent -0.82 (Kiørboe et al., 1990). The model gives a similar relation (Fig. 13), though with slower generation times. This may have to do with how the average generation time is calculated. In the model the generation time also includes cells with very slow DOC uptake rates, which increased the average generation time.

The modelled concentrations of labile DOC are very low (around 1 μM; Fig. 11b+g). This is because all DOC is considered labile and it is therefore immediately taken up and drawn down towards limiting concentrations which are around 0.1 μM (Fig. 6).

5.2 Effect of higher trophic level mortality

The model results depend upon the mortality exerted by the larger multicellular organisms as represented by the higher trophic level mortality μ_{htl}. The importance of the HTL mortality is not unique to size-based models; results of all plankton model are sensitive to this closure term. Varying the HTL mortality affects the size structure and the functions of the plankton ecosystem (Fig. 14). The main effect is to truncate the size-spectrum. The truncation releases the smaller plankton from predation and they respond by becoming more abundant. Due to this trophic cascade the total biomass and the net primary production are only weakly affected by the HTL mortality (Fig. 14b). The main effect is on the production towards the higher trophic levels, which has a uni-modal shape with a maximum at intermediate mortalities. This behaviour is similar to how fisheries models responds to fishing where the maximum is termed the "maximum sustainable yield". In lower productive system the effect of HTL mortality is stronger and the peak in HTL mortality is reached at lower mortalities (not shown).

Since the HTL mortality is an extrinsic parameter, we would like to know a reasonable value. That is difficult because the level of mortality depends on the predators: higher

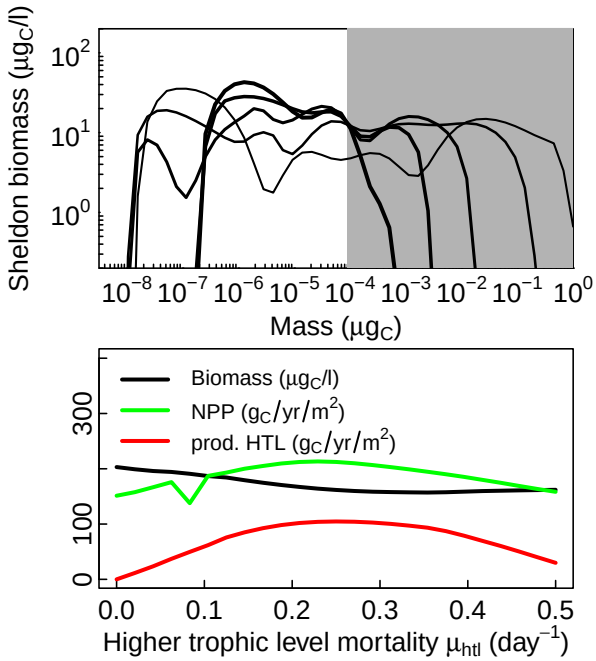

Figure 14: Effect of varying the mortality exerted by higher trophic levels from 0 to 0.5 day^{-1}. a) Sheldon size spectra; grey patch illustrates the size-range where HTL mortality acts. b) Effect of HTL mortality on ecosystem functions: total biomass, net primary production, and HTL productivity. Light and mixing are as the eutrophic situation Fig. 8

productivity of the larger plankton will lead to a higher HTL mortality. This effect is also seen inside the spectrum on the level of the predation mortality in Figs. 4.3-8b: in the oligotrophic system the level of mortality on the smallest plankton is around 0.1 day^{-1}rising to around 0.25 day^{-1}in the eutrophic system. HTL mortality should therefore not be higher than 0.25 day^{-1}. Here we have used 0.1 day^{-1}.

5.3 Effects of temperature

Water temperature directly affects affinities and metabolism, and through this, a host of processes from the division rate of cells, to ecosystem structure and functions (see Section 2.5; Fig. 15). Higher temperature increases the division rates of all cell sizes up to a point where division rates begin to decrease (panel b). The increase is relatively modest, though, and much less than indicated by a "metabolic" $Q_{10} = 2$, even for large heterotrophic cells. The decrease at higher temperature occurs when respiration losses, with a high Q_{10}, begins to dominate over the resource uptakes with smaller $Q'_{10}s$. The increasing division rates have a modest effect on ecosystem functions (panel b+c), but they act to increase the maximum size in the size spectrum. The declining division rates are reflected in lower productivities and lower spectra. The temperature response is, however, very dependent upon the conditions. Under oligotrophic conditions the temperature response is almost absent. The oligotrophic situation is dominated by carbon input from phototrophy (Fig. 8), which is independent of temperature ($Q_{10} = 1$). Furthermore, light is available in excess (dotted green line in Fig. 8b) and can easily support the basal metabolism. Clearly, the response to temperature depend on the mixing rate and light in complicated ways (Serra-Pompei et al., 2019) making it hard to make generalisations.

6 Discussion

We have developed a minimal first-principles approach to describe plankton community structure, dynamics and overall functions. The approach builds upon the central role of cell size for resource uptake and metabolism of unicellular plankton. By cultivating a view of each cell as a "generalist" that can perform all types of resource uptakes – essentially being a combination of a bacteria, a phytoplankton, and a zooplankton – the trophic strategies become an emergent property. The model therefore not only addresses the community size spectrum of the plankton community, but also the dominant trophic roles of plankton of different sizes. Particular novelties are the inclusion of dissolved organic carbon to represent carbon reuse and the microbial loop, and the development of closed-form analytical solutions for the extent, scaling, and level of the size-spectrum. Throughout we have maintained a focus on simplicity of all processes to bring forth a clear understanding of how each process contributes to the community structure. In the following we discuss how well first principles constrain the cell's function and which processes are still weakly constrained. Second, we discuss the limitations of the size-based approach to modelling plankton communities and how it relates to trait-based and functional-group based plankton models.

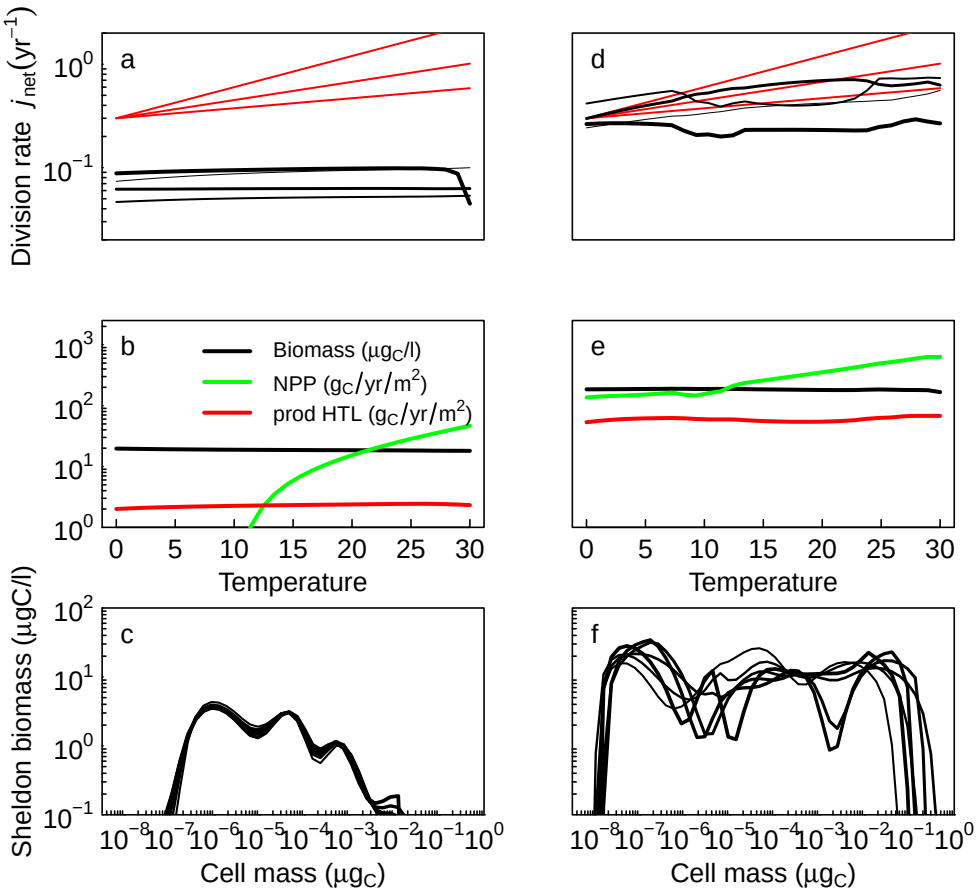

Figure 15: Effect of varying the temperature between 0 and 25 degrees in oligotrophic/eutrophic conditions (left/right columns; Fig. 8). a,d) Effect on the division rate j_{net} for 4 size classes (increasing line width). The red lines show temperature increases described by Q_{10} of 1.25, 1.5 and 2. b,e) Effect on ecosystem functions: total biomass, net primary production, and HTL productivity. c,f) spectra for 6 temperatures (increasing line widths).

6.1 Parameters from first principles, empirical relations, and tuning

"First principles" are relations rooted in physics and chemistry, or from geometry. Tying descriptions of processes and parameters to first principles has succeeded to varying degrees. Overall one can identify four levels of success: *i*) The process is known and the parameters can be calculated from first principles; *ii*) scaling exponents with cells size (mass, volume, or diameter) are known from first principles but the coefficients have to be calibrated with laboratory measurements or from meta-analyses; *iii*) The governing process is known, but the theoretical argument has not been developed and parameters rely solely on empirical knowledge; *iv*) The empirical evidence is lacking and parameters are only constrained indirectly via tuning of the outcome or loose arguments. For unicellular plankton all four levels are encountered.

The most complete level (*i*) description is how diffusion limits uptake of dissolved nutrient or DOC uptake and phototrophy, including the temperature scaling. For phototrophy there are clear theoretical arguments for all coefficients and scaling exponents – including the novel argument for the transition between two scaling regimes – simply from geometric arguments. However, a better understanding of the quantum yield is needed to fully describe the observed variation in light affinity. The other well known effect is how the cell wall limits the lower size of a cell, though the thickness of the cell wall is not (yet) constrained by first principle arguments. Another example of the role of geometry, which is not explored here, is the importance of a vacuole, a principle characteristic of diatoms, to modify the diffusion uptake (Hansen and Visser, 2019; Cadier et al., 2020). The other level (*i*) description is how clearance rate of prey encounter is derived from fluid mechanics, though it must be admitted that some approximation is needed to guesstimate the amount of energy available to the cell. As the fraction of energy only enters as a square root this value is not crucial. Comparing the theoretical result with data (Fig. 4) shows quite some scatter. It is known how the variation across the mean is due to the hydrodynamics of different flagella arrangements that also results in different predation risk (lower clearance leads to smaller predation risk; Nielsen and Kiørboe (2021)).

Most processes belong to the second level where scaling exponents are well described but empirical knowledge is needed to determine exact parameter values. To this category belong the processes related to surface limitations of resource uptake, passive exudation, and metabolism, including the temperature scaling of metabolism. The temperature dependence of metabolism is a complicated mixture of many different processes and a simple first-principles argument does not exist.

Finally, some of the parameters associated to DOC losses are largely guesswork (level iv). The poor state of knowledge is partly due to our limited understanding of the enormous diversity of DOC compounds and their lability which makes the lumping of DOC into one group crude.

Overall, while it is clear that first principles constrain cellular processes there is still room for improving the theoretical basis for estimation of some parameters.

6.2 Size-, trait-, and functional-group based plankton modelling

The central role of cell size for all vital processes makes it an obvious choice as the structuring variable for plankton community modelling. The community structure is then described as the "size spectrum" with the flat Sheldon spectrum being a typical solution. Here, this approach is taken further such that also the structure of the trophic strategies with cell size – on the continuum of osmo- photo- and heterotrophy (Andersen et al., 2015) – emerges as another dimension of the community structure. This idealized size-based approach has been demonstrated in a chemostat, a water column and in global simulations. The advantage of the pure size-based description is that the entire community, from the smallest bacteria to the largest heterotrophic cells, are captured with one set of parameters that is universal across geography and time. The obvious disadvantage is of course that biodiversity is only described by cell size and the dominant trophic strategy.

The size-based approach is closely related to a trait-based description of plankton (Kiørboe et al., 2018), with cell size being the only trait that is represented. As cell size can be considered the "master trait" the description of additional trait dimensions should also be related to cell size, such as investments in resource uptakes (Chakraborty et al., 2017) or reserves (Ho et al., 2020). Size-based models are essentially the simplest form of trait-based plankton models. The trait-distribution of other traits can be well represented by simply their optimal trait value (Chakraborty et al., 2020) or their moments (Bruggeman and Kooijman, 2007). The size spectrum itself, however, is continuous as shown in the analytical derivation of the Sheldon size spectrum. Descriptions of plankton where size is only reduced to its moment or the optimal size (Acevedo-Trejos et al., 2018, e.g.) may represent the changes of one group of plankton, but they are insufficient to resolve the entire community.

The traditional representation of plankton diversity is through dividing phyto- and zooplankton into functional groups, including picoplankton, diatoms, flagellates, ciliates, etc.. Functional group type models are powerful as the parameters in each group can be calibrated to represent the dominant group in a given study area to achieve good fits with observations of the different taxonomic groups. Their power comes at the expense of introducing additional parameters and by needing re-calibration if there are changes in the dominant species groups, as will happen when the environment changes. A good example of a functional-type model is the minimal plankton model of bacteria, auto- and heterotrophic flagellates, diatom, and copepods (Thingstad et al., 2007). The degree of complexity in terms of parameters is similar to a size-based model, but the model provides an explicit taxonomic resolution that is lacking in size-based models. Size-based models are not replacements of functional-group type models, but the two types of models should be considered as complementary descriptions of the same system. Therefore GCM-grade plankton models increasingly adopt descriptions that combine size and functional groups (Stock et al., 2014; Dutkiewicz et al., 2020, e.g.) to provide generality to functional-group type of models for global applications without inflating the parameter space.

6.3 Possibilities and problems of size-based plankton models

The simplicity of a size based description comes at the cost of ignoring important aspects of plankton diversity. Here we discuss the role of organism that increase their physical size without increasing carbon mass (diatoms and gelatinous zooplankton), alternative forms of nutrient uptakes (diazotrophs), and organisms with extreme predator-prey mass ratios (ciliates and larvaceans), and the difference between bacteria and eukaryotes.

Diatoms and gelatinous plankton increase their physical size by a large inert vacuole or a gelatinous body. In this way they gain the advantages of large physical size – higher nutrient uptake, higher photoharvesting rates, higher clearance rates, and lower average predation risk – without paying the cost of building and maintaining a large carbon mass. In a sense their success hinges on lowering their effective body density. The advantages of a lower body density follow directly from the size based relation developed here (Hansen and Visser, 2019), however, they are not explicitly represented in the model that is developed. Representing these life forms requires an additional trait, e.g. vacuole size (Cadier et al., 2020) or body density.

Diazotrophy is a dominant trophic strategy that is not represented in the simple size-based model. Diazotrophs fix nitrogen gas and thereby break away from the diffusion limitation on uptake of dissolved nitrogen. However, they still rely on diffusive uptakes of phosphorous and iron. Diazotrophy requires an oxygen-free environment, which requires the cell to limit the diffusion of oxygen into the cell. As the diffusion of oxygen into the cell follows the same size scaling as diffusive uptakes, it is challenging for small cells to develop diazotrophy, because they will have a high influx of oxygen. While the limitations of cell size on diazotrophy have not been described in the literature the fundamental understanding to develop it is available. With such a description, diazotrophy could be added directly as an additional process into the idealized size-based model.

Finally, the model assumes that all cells have the same preferred predator-prey mass. Some organisms, however, have very low predator-prey mass ratios, notably dinoflagellates (Kiørboe, 2008), while others have high ratios, notably larvaceans. The variation in preferred predator-prey masses is accommodated to some degree by using a prey size preference with a wide size range $\sigma > 1$. However, that solution poorly resolves the importance of organisms with large predator-prey masses in oligotrophic situations where they act to transfer carbon from the dominant picoplankton towards higher trophic levels. Not resolving higher predator-prey masses will underestimate the higher trophic level efficiency in oligotrophic situations.

Finally, the insistence on just one governing set of parameters for all sizes ignores the difference between bacteria and eukaryotes. Bacteria have a different cell wall structure which most likely limits their functional cell mass (the ν factor) less than in the description developed here. A proper distinction between bacteria and eukaryotes will also help make smaller cells more competitive such that the limiting resource level sizes (the R^*'s) will occur at smaller sizes.

Despite these reservations the "generalist" microbial model encompasses the governing principles to first order. It is the backbone on which to add other complications and the main effects seen in this minimal models will also be manifest in more complex size-based models. The importance of the additional complications – vacuoles, diazotrophy,

high predator-prey masses – can therefore be assessed with reference to the "generalist" size-based model.

Code

Code to generate all figures on github: https://github.com/Kenhasteandersen/FirstPrinciplesPlankton

Acknowledgements

Thanks to all the people who helped test and validate the models: Anton Almgren, Mathilde Cadier, Lisa Eckford-Soper, Trine Hansen, Amalia Papapostolou, and Camila Serra-Pompei. Special thanks to Saeed Asadzadeh for discussions about the scaling of clearance rate with size. This work was supported by the VKR Center of Excellence Ocean Life, the Gordon and Betty Moore foundation, and the European Union's Horizon 2020 research and innovation programme under grant agreement No. 869383 (ECOTIP).

References

Acevedo-Trejos, E., E. Marañón, and A. Merico (2018). Phytoplankton size diversity and ecosystem function relationships across oceanic regions. *Proceedings of the Royal Society B: Biological Sciences 285*(1879), 20180621. ZSCC: 0000030 Publisher: The Royal Society.

Aksnes, D. L. and J. K. Egge (1991). A theoretical model for nutrient uptake in phytoplankton. *Marine ecology progress series. Oldendorf 70*(1), 65–72.

Andersen, K., D. L. Aksnes, T. Berge, O. Fiksen, and A. Visser (2015). Modelling emergent trophic strategies in plankton. *Journal of Plankton Research 37*(5), 862–868.

Andersen, K., T. Berge, R. J. Gonçalves, M. Hartvig, J. Heuschele, S. Hylander, N. S. Jacobsen, C. Lindemann, E. A. Martens, A. B. Neuheimer, K. Olsson, A. Palacz, F. Prowe, J. Sainmont, S. J. Traving, A. W. Visser, N. Wadhwa, and T. Kiørboe (2016). Characteristic sizes of life in the oceans, from bacteria to whales. *Annual Review of Marine Science 8*, 217–241.

Andersen, K. H. and J. E. Beyer (2006). Asymptotic Size Determines Species Abundance in the Marine Size Spectrum. *The American Naturalist 168*(1), 54–61.

Anderson, T. R. (2005). Plankton functional type modelling: running before we can walk? *Journal of plankton research 27*(11), 1073–1081. ISBN: 1464-3774 Publisher: Oxford University Press.

Anderson, T. R., W. C. Gentleman, and A. Yool (2015). EMPOWER-1.0: an efficient model of planktonic ecosystems written in R. *Geoscientific Model Development 8*(7), 2231–2262. ISBN: 1991-9603.

Anderson, T. R. and P. l. B. Williams (1998). Modelling the seasonal cycle of dissolved organic carbon at Station E1in the English Channel. *Estuarine, Coastal and Shelf Science 46*(1), 93–109. ZSCC: 0000140 ISBN: 0272-7714 Publisher: Elsevier.

Armstrong, R. A. (1994). Grazing limitation and nutrient limitation in marine ecosystems: steady state solutions of an ecosystem model with multiple food chains. *Limnology and Oceanography 39*(3), 597–608. ISBN: 0024-3590 Publisher: Wiley Online Library.

Armstrong, R. A. (2008). Nutrient uptake rate as a function of cell size and surface transporter density: a Michaelis-like approximation to the model of Pasciak and Gavis. *Deep Sea Research Part I: Oceanographic Research Papers 55*(10), 1311–1317. ISBN: 0967-0637 Publisher: Elsevier.

Baird, M. E. and I. M. Suthers (2007). A size-resolved pelagic ecosystem model. *Ecological Modelling 203*(3-4), 185–203. ZSCC: 0000100 Publisher: Elsevier.

Banas, N. S. (2011). Adding complex trophic interactions to a size-spectral plankton model: Emergent diversity patterns and limits on predictability. *Ecological Modelling 222*(15), 2663–2675.

Berg, H. C. and E. M. Purcell (1977). Physics of chemoreception. *Biophysical Journal 20*, 193–219.

Bjørnsen, P. K. (1988). Phytoplankton exudation of organic matter: Why do healthy cells do it? *Limnology and oceanography 33*(1), 151–154. ZSCC: 0000330 Publisher: Wiley Online Library.

Boudreau, P. R. and L. M. Dickie (1992). Biomass spectra of aquatic ecosystems in relation to fisheries yield. *Canadian Journal of Fisheries and Aquatic Sciences 49*(8), 1528–1538. Publisher: NRC Research Press Ottawa, Canada.

Braakman, R., M. J. Follows, and S. W. Chisholm (2017). Metabolic evolution and the self-organization of ecosystems. *Proceedings of the National Academy of Sciences 114*(15), E3091–E3100. ZSCC: 0000102 Publisher: National Acad Sciences.

Bruggeman, J. and S. A. L. M. Kooijman (2007). A biodiversity-inspired approach to aquatic ecosystem modeling. *Limnology and Oceanography 52*(4), 1533–1544.

Cadier, M., A. N. Hansen, K. H. Andersen, and A. W. Visser (2020). Competition between vacuolated and mixotrophic unicellular plankton. *Journal of Plankton Research 42*(4), 425–439. ISBN: 0142-7873 Publisher: Oxford University Press.

Carlson, C. (2002). Production and removal processes. In *Biogeochemistry of marine dissolved organic matter*, pp. 91–151.

Chakraborty, S., M. Cadier, A. W. Visser, J. Bruggeman, and K. H. Andersen (2020). Latitudinal variation in plankton traits and ecosystem function. *Global Biogeochemical Cycles e2020GB006564*, 1–25.

Chakraborty, S., L. Nielsen, and K. H. Andersen (2017). Trophic strategies of unicellular plankton. *American Naturalist 189*(4), E77–E90.

Dutkiewicz, S., P. Cermeno, O. Jahn, M. J. Follows, A. E. Hickman, D. A. Taniguchi, and B. A. Ward (2020). Dimensions of marine phytoplankton diversity. *Biogeosciences 17*(3), 609–634. ZSCC: 0000051 ISBN: 1726-4170 Publisher: Copernicus GmbH.

Duyens, L. N. M. (1956). The flattening of the absorption spectrum of suspensions, as compared to that of solutions. *Biochimica et Biophysica Acta 19*, 1–12. ZSCC: NoCitationData[s0].

Edwards, K. F., C. A. Klausmeier, and E. Litchman (2015). Nutrient utilization traits of phytoplankton: ecological archives E096-202. *Ecology 96*(8), 2311–2311. ISBN: 1939-9170 Publisher: Wiley Online Library.

Edwards, K. F., M. K. Thomas, C. A. Klausmeier, and E. Litchman (2012). Allometric scaling and taxonomic variation in nutrient utilization traits and maximum growth rate of phytoplankton. *Limnology and Oceanography 57*(2), 554–566.

Edwards, K. F., M. K. Thomas, C. A. Klausmeier, and E. Litchman (2015). Light and growth in marine phytoplankton: allometric, taxonomic, and environmental variation. *Limnology and Oceanography 60*(2), 540–552. ISBN: 0024-3590 Publisher: Wiley Online Library.

Evans, G. T. and J. S. Parslow (1985). A model of annual plankton cycles. *Biological oceanography 3*(3), 327–347.

Fasham, M. J. R., H. W. Ducklow, and S. M. McKelvie (1990). A nitrogen-based model of plankton dynamics in the oceanic mixed layer. *Journal of Marine Research 48*(3), 591–639.

Fenchel, T. (1987). *Ecology of Protozoa: The biology of free-living phagotropic protists*. Springer-Verlag. ZSCC: NoCitationData[s0].

Fiksen, O., M. J. Follows, and D. L. Aksnes (2013). Trait-based models of nutrient uptake in microbes extend the Michaelis-Menten framework. *Limnology and Oceanography 58*(1), 193–202.

Finkel, Z. V., J. Beardall, K. J. Flynn, A. Quigg, T. A. V. Rees, and J. a. Raven (2010). Phytoplankton in a changing world: Cell size and elemental stoichiometry. *Journal of Plankton Research 32*(1), 119–137.

Flynn, K. J., D. R. Clark, and Y. Xue (2008). Modeling the release of dissolved organic matter by phytoplankton 1. *Journal of phycology 44*(5), 1171–1187. ZSCC: 0000048 ISBN: 0022-3646 Publisher: Wiley Online Library.

Franks, P. J. (2002). NPZ models of plankton dynamics: their construction, coupling to physics, and application. *Journal of Oceanography 58*(2), 379–387. ISBN: 0916-8370 Publisher: Springer.

Franks, P. J. S. (2009). Planktonic ecosystem models: perplexing parameterizations and a failure to fail. *Journal of Plankton Research 31*(11), 1299–1306.

Haldane, J. B. (1926). On being the right size. *Harper's Magazine 152*, 424–427.

Hansen, A. N. and A. W. Visser (2019). The seasonal succession of optimal diatom traits. *Limnology and Oceanography 64*(4), 1442–1457.

Hansen, B., P. K. Bjørnsen, and P. J. Hansen (1994). The size ratio between planktonic predators and their prey. *Limnology and Oceanography 39*(2), 395–403.

Hillebrand, H., E. Acevedo-Trejos, S. D. Moorthi, A. Ryabov, M. Striebel, P. Thomas, and M.-L. Schneider (2021). Cell size as driver and sentinel of phytoplankton community structure and functioning. *Functional Ecology 00*, 1–18. ZSCC: 0000001 Publisher: Wiley Online Library.

Hirst, A. G. and T. Kiørboe (2002). Mortality of marine planktonic copepods: global rates and patterns. *Marine Ecology Progress Series 230*, 195–209.

Ho, P.-C., C.-W. Chang, F.-K. Shiah, P.-L. Wang, C.-h. Hsieh, and K. H. Andersen (2020). Body size, light intensity, and nutrient supply determine plankton stoichiometry in mixotrophic plankton food webs. *The American Naturalist 195*(4), E100–E111. ISBN: 0003-0147 Publisher: The University of Chicago Press Chicago, IL.

Hood, R. R., E. A. Laws, R. A. Armstrong, N. R. Bates, C. W. Brown, C. A. Carlson, F. Chai, S. C. Doney, P. G. Falkowski, and R. A. Feely (2006). Pelagic functional group modeling: Progress, challenges and prospects. *Deep Sea Research Part II: Topical Studies in Oceanography 53*(5-7), 459–512. ZSCC: 0000232 Publisher: Elsevier.

Jumars, P. A., J. W. Deming, P. S. Hill, L. Karp-Boss, P. L. Yager, and W. B. Dade (1993). Physical constraints on marine osmotrophy in an optimal foraging context. *Aquatic Microbial Ecology 7*(2), 121–159.

Khatiwala, S. (2007). A computational framework for simulation of biogeochemical tracers in the ocean. *Global Biogeochemical Cycles 21*(3), GB3001.

Khatiwala, S., M. Visbeck, and M. A. Cane (2005). Accelerated simulation of passive tracers in ocean circulation models. *Ocean Modelling 9*(1), 51–69.

Kirchman, D. L. (2010). *Microbial ecology of the oceans*, Volume 36. John Wiley & Sons.

Kirk, J. T. O. (1975). A theoretical analysis of the contribution of algal cells to the attenuation of light within natural waters II. spherical cells. *New Phytologist 75*(1), 21–36. ZSCC: 0000188.

Kishino, M., N. Okami, M. Takahashi, and S.-e. Ichimura (1986). Light utilization efficiency and quantum yield of phytoplankton in a thermally stratified sea 1. *Limnology and Oceanography 31*(3), 557–566. Publisher: Wiley Online Library.

Kiørboe, T. (1993). Turbulence, phytoplankton cell size, and the structure of pelagic food webs. *Adv. Mar. Biol. 29*, 1–72.

Kiørboe, T. (2008). *A mechanistic approach to plankton ecology*. Princeton University Press.

Kiørboe, T. (2011). How zooplankton feed: mechanisms, traits and trade-offs. *Biological reviews of the Cambridge Philosophical Society 86*(2), 311–39.

Kiørboe, T. (2013). Attack or Attacked: The Sensory and Fluid Mechanical Constraints of Copepods' Predator-Prey Interactions. *Integrative and comparative biology 53*(5), 821–831.

Kiørboe, T. and A. G. Hirst (2014). Shifts in mass scaling of respiration, feeding, and growth rates across life-form transitions in marine pelagic organisms. *The American naturalist 183*(4), E118–30.

Kiørboe, T., H. Kaas, B. Kruse, F. Møhlenberg, P. Tiselius, and G. Ærtebjerg (1990). The structure of the pelagic food web in relation to water column structure in the Skagerrak. *Marine Ecology Progress Series 59*, 19–32.

Kiørboe, T., A. Visser, and K. H. Andersen (2018). A trait-based approach to ocean ecology. *ICES Journal of Marine Science 75*(6), 1849–1863.

Klausmeier, C. A. and E. Litchman (2001). Algal games: The vertical distribution of phytoplankton in poorly mixed water columns. *Limnology and Oceanography 46*(8), 1998–2007.

Kriest, I. and A. Oschlies (2007). Modelling the effect of cell-size-dependent nutrient uptake and exudation on phytoplankton size spectra. *Deep Sea Research Part I: Oceanographic Research Papers 54*(9), 1593–1618. ZSCC: 0000019 ISBN: 0967-0637 Publisher: Elsevier.

López-Sandoval, D. C., T. Rodríguez-Ramos, P. Cermeño, and E. Marañón (2013). Exudation of organic carbon by marine phytoplankton: dependence on taxon and cell size. *Marine ecology progress series 477*, 53–60. ZSCC: 0000037 ISBN: 0171-8630.

Maranón, E., P. Cermeno, E. Fernández, J. Rodríguez, and L. Zabala (2004). Significance and mechanisms of photosynthetic production of dissolved organic carbon in a coastal eutrophic ecosystem. *Limnology and Oceanography 49*(5), 1652–1666. ZSCC: 0000122 ISBN: 0024-3590 Publisher: Wiley Online Library.

Marañón, E. (2015). Cell size as a key determinant of phytoplankton metabolism and community structure. *Annual review of marine science 7*, 241–264.

Menden-Deuer, S. and E. J. Lessard (2000). Carbon to volume relationships for dinoflagellates, diatoms, and other protist plankton. *Limnology and oceanography 45*(3), 569–579. ISBN: 0024-3590 Publisher: Wiley Online Library.

Moloney, C. L. and J. G. Field (1989). General allometric equations for rates of nutrient uptake, ingestion, and respiration in plankton organisms. *Limnology and Oceanography 34*(7), 1290–1299.

Morel, A. and A. Bricaud (1981). Theoretical results concerning light absorption in a discrete medium, and application to specific absorption of phytoplankton. *Deep Sea Research 28*(11), 1375–1393.

Negrete-García, G., J. Y. Luo, M. C. Long, K. Lindsay, M. Levy, and A. D. Barton (2022). Plankton energy flows using a global size-structured and trait-based model. *Bioarxiv*, 1–70.

Nielsen, L. T., S. S. Asadzadeh, J. Dölger, J. H. Walther, T. Kiørboe, and A. Andersen (2017, August). Hydrodynamics of microbial filter feeding. *Proceedings of the National Academy of Sciences 114*(35), 9373–9378.

Nielsen, L. T. and T. Kiørboe (2021). Foraging trade-offs, flagellar arrangements, and flow architecture of planktonic protists. *Proceedings of the National Academy of Sciences 118*(3), 1–6. ZSCC: 0000002 ISBN: 0027-8424 Publisher: National Acad Sciences.

Okie, J. G., V. H. Smith, and M. Martin-Cereceda (2016). Major evolutionary transitions of life, metabolic scaling and the number and size of mitochondria and chloroplasts. *Proceedings of the Royal Society B: Biological Sciences 283*(1831), 20160611. ZSCC: 0000025 Publisher: The Royal Society.

Palmer, J. R. and I. J. Totterdell (2001). Production and export in a global ocean ecosystem model. *Deep Sea Research Part I: Oceanographic Research Papers 48*(5), 1169–1198. ZSCC: 0000265 Publisher: Elsevier.

Pasciak, W. J. and J. Gavis (1974). Transport limitation of nutrient uptake in phytoplankton 1. *Limnology and Oceanography 19*(6), 881–888. ISBN: 0024-3590 Publisher: Wiley Online Library.

Payne, J. L., C. R. McClain, A. G. Boyer, J. H. Brown, S. Finnegan, M. Kowalewski, R. A. Krause, S. K. Lyons, D. W. McShea, and P. M. Novack-Gottshall (2011). The evolutionary consequences of oxygenic photosynthesis: a body size perspective. *Photosynthesis research 107*(1), 37–57. ZSCC: 0000081 Publisher: Springer.

Quere, C. L., S. P. Harrison, I. Colin Prentice, E. T. Buitenhuis, O. Aumont, L. Bopp, H. Claustre, L. Cotrim Da Cunha, R. Geider, and X. Giraud (2005). Ecosystem dynamics based on plankton functional types for global ocean biogeochemistry models. *Global Change Biology 11*(11), 2016–2040.

Raven, J. A. (1984). A cost-benefit analysis of photon absorption by photosynthetic unicells. *New Phytologist 98*(4), 593–625.

Raven, J. A. (1994). Why Are There No Picoplanktonic O$_2$ Evolvers with Volumes Less Than $10^-{19}$ m^3? *Journal of Plankton Research 16*, 565–580.

Raven, J. A. (1997). The vacuole: a cost-benefit analysis. In *Advances in Botanical Research*, Volume 25, pp. 59–86. Elsevier. ZSCC: 0000081.

Rose, J. M. and D. A. Caron (2007). Does low temperature constrain the growth rates of heterotrophic protists? Evidence and implications for algal blooms in cold waters. *Limnology and Oceanography 52*(2), 886–895. ZSCC: 0000301 ISBN: 0024-3590 Publisher: Wiley Online Library.

Ryther, J. H. (1969). Photosynthesis and fish production in the sea. *Science 166*(3901), 72–76.

Serra-Pompei, C., G. I. Hagstrom, A. W. Visser, and K. H. Andersen (2019). Resource limitation determines temperature response of unicellular plankton communities. *Limnology and Oceanography 64*(4), 1627–1640.

Sheldon, R. W., A. Prakash, and W. Sutcliffe Jr (1972). The size distribution of particles in the ocean. *Limnology and oceanography 17*(3), 327–340.

Shuter, B. (1979). A Model of Physiological Adaptation in Unicellular Algae. *Journal of Theoretical Biology 78*, 519–552.

Sprules, W. and L. Barth (2016). Surfing the biomass size spectrum: some remarks on history, theory, and application. *Canadian Journal of Fisheries and Aquatic Sciences 73*(4), 477–495.

Stammer, D., K. Ueyoshi, A. Köhl, W. G. Large, S. A. Josey, and C. Wunsch (2004). Estimating air-sea fluxes of heat, freshwater, and momentum through global ocean data assimilation. *Journal of Geophysical Research: Oceans 109*(C05023), 1–16. ZSCC: 0000193 Publisher: Wiley Online Library.

Stock, C. A., J. P. Dunne, and J. G. John (2014). Global-scale carbon and energy flows through the marine planktonic food web: An analysis with a coupled physical-biological model. *Progress in Oceanography 120*, 1–28.

Stock, C. A., J. G. John, R. R. Rykaczewski, R. G. Asch, W. W. Cheung, J. P. Dunne, K. D. Friedland, V. W. Lam, J. L. Sarmiento, and R. A. Watson (2017). Reconciling fisheries catch and ocean productivity. *Proceedings of the National Academy of Sciences 114*(8), E1441–E1449.

Stock, C. A., T. M. Powell, and S. A. Levin (2008). Bottom–up and top–down forcing in a simple size-structured plankton dynamics model. *Journal of Marine Systems 74*(1-2), 134–152.

Taguchi, S. (1976). Relationship between photosynthesis and cell size of marine diatoms. *Journal of Phycology 12*(2), 185–189.

Teira, E., M. José Pazó, P. Serret, and E. Fernández (2001). Dissolved organic carbon production by microbial populations in the Atlantic Ocean. *Limnology and Oceanography 46*(6), 1370–1377. ZSCC: 0000130 ISBN: 0024-3590 Publisher: Wiley Online Library.

Terseleer, N., J. Bruggeman, C. Lancelot, and N. Gypens (2014). Trait-based representation of diatom functional diversity in a plankton functional type model of the eutrophied southern North Sea. *Limnology and Oceanography 59*(6), 1958–1972.

Thingstad, T. F., H. Havskum, U. L. Zweifel, E. Berdalet, M. M. Sala, F. Peters, M. Alcaraz, R. Scharek, M. Perez, and S. Jacquet (2007). Ability of a "minimum" microbial food web model to reproduce response patterns observed in mesocosms manipulated with N and P, glucose, and Si. *Journal of Marine Systems 64*(1-4), 15–34. ZSCC: 0000038 Publisher: Elsevier.

Thornton, D. C. (2014). Dissolved organic matter (DOM) release by phytoplankton in the contemporary and future ocean. *European Journal of Phycology 49*(1), 20–46. ZSCC: 0000208 ISBN: 0967-0262 Publisher: Taylor & Francis.

Tilman, D. (1982). Resource competition and community structure. *Monographs in population biology 17*, 1–296.

Van Oostende, N., R. Dussin, C. A. Stock, A. D. Barton, E. Curchitser, J. P. Dunne, and B. B. Ward (2018). Simulating the ocean's chlorophyll dynamic range from coastal upwelling to oligotrophy. *Progress in oceanography 168*, 232–247. ZSCC: NoCitationData[s0] Publisher: Elsevier.

Ward, B. and M. J. Follows (2016). Marine mixotrophy increases trophic transfer efficiency, mean organism size, and vertical carbon flux. *Proceedings of the National Academy of Sciences 113*(11), 201517118.

Ward, B. A., E. Marañón, B. Sauterey, J. Rault, and D. Claessen (2016, December). The Size Dependence of Phytoplankton Growth Rates: A Trade-Off between Nutrient Uptake and Metabolism. *The American Naturalist 189*(2), 170–177.

Ward, B. A., J. D. Wilson, R. M. Death, F. M. Monteiro, A. Yool, and A. Ridgwell (2018). EcoGEnIE 1.0: plankton ecology in the cGEnIE Earth system model. *Geoscientific Model Development 11*(10), 4241–4267. ISBN: 1991-9603.

Zwanzig, R. (1990). Diffusion-controlled ligand binding to spheres partially covered by receptors: an effective medium treatment. *Proceedings of the National Academy of Sciences 87*(15), 5856–5857. Publisher: National Acad Sciences.

A Calculation of effective prey preference for discrete size groups

The effective prey preferences function between size groups of predators i and prey j is calculated by integrating over the prey size preference (26). The encountered prey in size group j by all predators in group i is:

$$E_{ij} = \int_{m_i^-}^{m_i^+} a_{\mathrm{F}} m \int_{m_j^-}^{m_j^+} \phi(m,\, w) B(w)\, \mathrm{d}w\, B(m)/m\, \mathrm{d}m. \tag{A.1}$$

Here, $B(m)$ represents the normalized biomass spectrum. We assume a Sheldon distribution, i.e., $B(m) \propto m^{-1}$. With the discrete prey and predator groups we write the encountered food as:

$$E_{ij} = a_{\mathrm{F}} m_i \Phi_{ij} B_j N_i \tag{A.2}$$

Where B_j is the total biomass in group j, $B_j = \int B(w)\, \mathrm{d}w$ and N_i is the total abundance of predators $N_i = \int B(m)/m\, \mathrm{d}m$. Equating the two terms and isolating Φ_{ij} gives:

$$\begin{aligned}\Phi_{ij} = \frac{\sqrt{\Delta}}{(\Delta - 1)\log(\Delta)} & \\ \Bigg[\Bigg(\frac{1}{2} s \left(e^{-\frac{\log^2\left(\frac{\Delta z}{\beta}\right)}{s}} + e^{-\frac{\log^2\left(\frac{\beta\Delta}{z}\right)}{s}} - 2e^{-\frac{\log^2\left(\frac{z}{\beta}\right)}{s}}\right) - & \\ \frac{1}{2}\sqrt{\pi}\sqrt{s}\left(\log\left(\frac{\Delta z}{\beta}\right) \operatorname{erf}\left(\frac{\log(\beta) - \log(\Delta z)}{\sqrt{s}}\right) + \log\left(\frac{\beta\Delta}{z}\right) \operatorname{erf}\left(\frac{\log(z) - \log(\beta\Delta)}{\sqrt{s}}\right) + & \\ \log\left(\frac{z}{\beta}\right) \operatorname{erf}\left(\frac{\log\left(\frac{z}{\beta}\right)}{\sqrt{s}}\right)\Bigg)\Bigg)\Bigg] & \end{aligned} \tag{A.3}$$

where $s = 2\sigma^2$ and $z = m_i/m_j$ and $\Delta = m^+/m^-$.

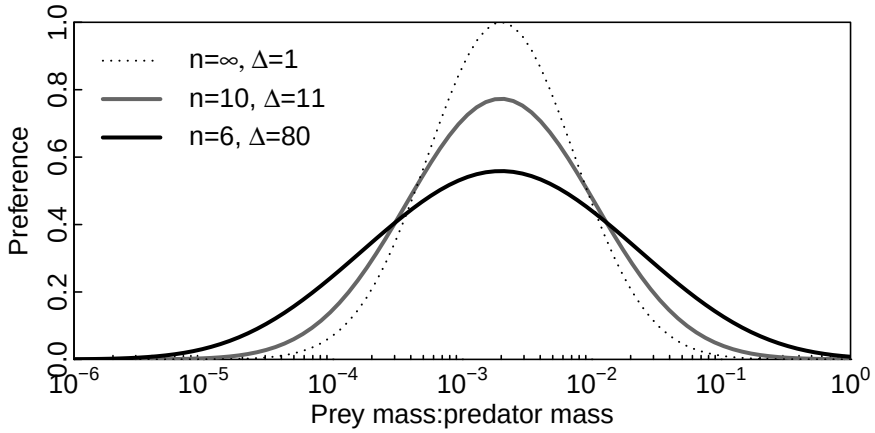

Figure A.1: Size preference function for different grid expansions (Δ) and number of size groups (n).